

Fluid Flow in Cylindrical Ducts with Nanoparticles

by

Saira Asghar

A thesis submitted in partial fulfillment of the requirements for the
degree of Master of Science in Mathematics




Supervised by

Dr. Moniba Shams

School of Natural Sciences (SNS),
National University of Sciences and Technology,
H-12, Islamabad, Pakistan

National University of Sciences & Technology**MASTER'S THESIS WORK**

We hereby recommend that the dissertation prepared under our supervision by: Saira Asghar, Regn No. 00000278471 Titled: Fluid Flow in Cylindrical Ducts with Nanoparticles be accepted in partial fulfillment of the requirements for the award of **MS** degree.

Examination Committee Members1. Name: DR. M. ASIF FAROOQSignature: 2. Name: DR. HINA SADAFSignature: External Examiner: DR. NABEELA KAUSARSignature: Supervisor's Name: DR. MONIBA SHAMSSignature: 


Head of Department

03/09/2021
Date

COUNTERSIGNEDDate: 3.9.2021


Dean/Principal

Dedicated
to
My Beloved Parents

Acknowledgements

All praises be to Allah, the Lord of the world, the Master of the Day After, who has given unlimited mercy to His creations which show Allah's love is spread around. Peace and salutation are uttered to beloved Prophet Muhammad SAW (peace upon him) who has brought mankind from wickedness to the truth of Islam.

I feel great pleasure in expressing my profound and heartiest gratitude to my respected supervisor **Dr. Moniba Shams**, for her indispensable guidance, encouragement and active co-operation that made possible this work to meet its end successfully. May Allah shower his countless blessing upon them and bless her with good health and knowledge. I would like to pay my gratitude to my GEC members **Dr. Muhammad Asif Farooq** and **Dr. Hina Sadaf** for their support and guidance in completing this thesis.

I owe my respect and gratitude to my father **Asghar Ali**, my mother **Naseem Begum**, my siblings and my grandparents. Their endless love, prayers and encouragement have always been a source of strength for me. Sincere thanks to all my friends for their kindness and moral support during my study. Finally, thanks to my all class fellows for their prayers and co-ordination.

Saira Asghar

Abstract

In present dissertation, two papers are discussed. Firstly, the magneto-hydrodynamics (MHD) movement of copper (Cu) nanoparticles under the action of water with an oscillating pressure gradient among two concentric ducts is reviewed. Nanoparticles addition is assumed to have significantly improved thermal performance near surface for turbulent and laminar flow. The standard governing equations are partial differential equations and comprises effective thermal conductivity, base fluid viscosity and thermophysical characteristics of water based Cu nanoparticles. The exact solutions are obtained in the form of the modified Bessel functions of first and second kind. Pressure difference, vorticity, temperature and velocity distribution are analyzed graphically for several flow controlling parameters. Outcomes affirmed that velocity, temperature and heat transfer rate can be modified with the help of external magnetic field and nanoparticles addition. Secondly, considering the magnetic field, the flow and heat transfer of nanofluids through a stretching cylinder is discussed. A similarity solution is suggested, which transforms the constitutive equations into the set of ODEs. Various type of nanoparticles like alumina (Al_2O_3), copper (Cu), silver (Ag), and titanium oxide (TiO_2) are considered, alongwith water (H_2O) as a base fluid. Significant fluid dynamics concepts such as heat transfer rate, skin friction coefficient, velocity distribution, Nusselt number etc. are analyzed and plotted graphically. Furthermore,

radiation effects on heat transfer and MHD flow of nanofluids in a porous medium is analyzed. The solution of the system of equations is evaluated numerically by MATLAB function *bvp4c*. The impact of flow controlling parameters like heat generation or absorption parameter (Q), porosity parameter (K), thermal radiation (Nr), and volume fraction (ϕ) on temperature and velocity profiles for Cu-water nanoparticles are investigated. The graphical and tabular results demonstrates that these parameters provide a remarkable change in Nusselt number and skin friction coefficient.

Contents

Nomenclature	x
List of figures	xiii
List of tables	xvi
1 Introduction	1
2 Preliminaries and basic concepts	8
2.1 Fluid and fluid flows	8
2.2 Compressible and incompressible flows	8
2.3 Laminar and turbulent flows	9
2.4 Steady and unsteady flows	9
2.5 Pulsatile flow	10
2.6 Newtonian and non-Newtonian fluids	10
2.7 Axi-symmetric flow	10
2.8 Viscosity	10
2.9 Conservation laws	11

2.9.1	Continuity equation	11
2.9.2	Momentum equation	12
2.9.3	Energy equation	12
2.10	Porous medium	13
2.11	Vortex	13
2.12	Boundary conditions	13
2.12.1	Slip condition	14
2.12.2	No-slip condition	14
2.13	Magnetohydrodynamics	14
2.14	Heat transfer mechanism	15
2.14.1	Convection	15
2.14.2	Radiation	16
2.14.3	Conduction	16
2.15	Boundary layer	17
2.16	Skin friction coefficient	17
2.17	Dimensionless parameters	17
2.17.1	Reynolds number	17
2.17.2	Nusselt number	18
2.17.3	Hartmann number	18
2.17.4	Prandtl number	19
2.18	Nanofluids	19
2.19	Thermophysical properties of nanofluid	19
2.19.1	Specific Heat	19

2.19.2	Density	20
2.19.3	Dynamic viscosity	20
2.19.4	Thermal conductivity	20
2.19.5	Electrical conductivity	21
3	Water driven copper nanoparticles between two concentric cylinders with an oscillatory pressure gradient	22
3.1	Problem formulation	22
3.2	Solution of the problem	28
3.2.1	Pressure	30
3.3	Graphical analysis	31
3.3.1	Velocity	32
3.3.2	Vortex	40
3.3.3	Pressure	42
3.3.4	Temperature	43
4	Heat transfer and nanofluids MHD flow across stretching cylinder	47
4.1	bvp4c	47
4.2	Mathematical formulation	48
4.3	Numerical method	52
4.4	Results and discussion	54
4.4.1	Velocity	55
4.4.2	Temperature	56
4.4.3	Skin friction coefficient and Nusselt number	58

5	Darcy and radiation effect on heat transfer and MHD nanofluid flow across stretching cylinder	63
5.1	Introduction	63
5.2	Mathematical formulation	64
5.3	Numerical method	70
5.4	Results and discussion	71
5.4.1	Velocity	71
5.4.2	Temperature	73
5.4.3	Skin friction coefficient and Nusselt number	76
6	Concluding Remarks	80
6.1	Water driven copper nanoparticles between two concentric cylinders with an oscillatory pressure gradient	80
6.2	Heat transfer and nanofluids MHD flow across stretching cylinder . . .	81
6.3	Darcy and radiation effect on heat transfer and MHD nanofluid flow across stretching cylinder	81
	Bibliography	82
	Appendix	89

Nomenclature

ρ	Density.
ρ_{nf}	Nanofluid density.
ρ_p	Density of nanoparticles.
ρ_f	Fluid density.
μ	Viscosity.
c	Specific heat.
ν	Kinematic viscosity.
A	Amplitude.
σ	Electrical conductivity.
r_e	External radius of outer cylinder.
r_i	Internal radius of inner cylinder.
p	Pressure.
κ	Thermal conductivity.

T	Temperature.
a^*	Cylinder radius.
q_w	Heat transfer from cylinder surface.
T_w	Temperature of cylinder surface.
T_∞	Ambient temperature.
\vec{B}	Magnetic field.
\vec{J}	Current density.
L	Length of cylinder.
t	Time.
σ^*	Stefan-Boltzmann constant.
k^*	Mean absorption.
K_o	Permeability.
b	Positive constant.
u, v, w	Velocity components.
Pr	Prandtl number.
C_f	Skin friction coefficient .
M	Magnetic parameter.
τ_w	Wall shear stress.

η	Similarity variable.
Nu	Nusselt number.
ϕ	Nanoparticle volume fraction.
θ	Similarity function for temperature.
Re	Reynolds number.
q_r	Radiative heat flux.
Q	Heat generation/absorption parameter.
Nr	Radiation parameter.

Subscripts

w	Condition at surface.
∞	Far field.
f	Fluid.
nf	Nanofluid.
s	Solid nanoparticles.
i	Internal.
e	External.
p	Particle.

List of Figures

3.1	Flow field geometry.	23
3.2	Velocity profile variance for $0^\circ \leq t \leq 360^\circ$ when $Re = 1$ and $M = 0$. . .	33
3.3	Velocity profile variance for $0^\circ \leq t \leq 360^\circ$ when $Re = 100$ and $M = 0$.	34
3.4	Velocity profile variance for $0^\circ \leq t \leq 360^\circ$ when $Re = 900$ and $M = 0$. .	35
3.5	Velocity profile variance for $0^\circ \leq t \leq 360^\circ$ when $Re = 1$ and $M = 10$. .	36
3.6	Velocity profile variance for $0^\circ \leq t \leq 360^\circ$ when $Re = 30$ and $M = 30$. .	37
3.7	For base fluid, R^* influence on velocity profile when $Re = 400$ and $t = 30$.	38
3.8	R^* influence on velocity profile for different ϕ when $Re = 400$ and $t = 30$.	39
3.9	For base fluid, variance in vortex profile for $0^\circ \leq t \leq 360^\circ$ when $M = 5$ and $Re = 100$	40
3.10	For different ϕ variance in vortex profile for $0^\circ \leq t \leq 360^\circ$ when $M = 5$ and $Re = 100$	41
3.11	Pressure gradient at $R^* = 0.2$ when $Re = 100$ and $M = 30$	42
3.12	Pressure gradient at $R^* = 0.4$ when $Re = 100$ and $M = 30$	42
3.13	Pressure gradient (A) influence on temperature profile.	43
3.14	Pressure gradient (A) influence on temperature profile.	44
3.15	Nanoparticle volume fraction (ϕ) influence on temperature profile.	45

3.16 (a) Hartmann number and (b-c) time influence on temperature profile.	46
4.1 Physical configuration and coordinate system.	49
4.2 Variations in velocity distribution against ϕ	55
4.3 Variations in velocity distribution against M	56
4.4 Temperature profile variance against ϕ	57
4.5 Temperature profile variance against M	57
4.6 Temperature distribution for different nanofluids.	58
4.7 ϕ and M influence on skin friction coefficient.	59
4.8 ϕ and Re influence on skin friction coefficient.	59
4.9 ϕ and Re Influence on Nusselt number.	60
4.10 ϕ and M Influence on Nusselt number.	60
5.1 Physical model and coordinate system.	64
5.2 Velocity profile against porosity parameter.	72
5.3 Velocity profile against M	72
5.4 Velocity profile against varying choice of ϕ	73
5.5 Temperature profile against M	74
5.6 Temperature profile against Q	74
5.7 Temperature profile against Nr	75
5.8 Temperature profile against ϕ	75
5.9 K and ϕ influence on skin friction coefficient.	76
5.10 ϕ and Q influence on skin friction coefficient.	77
5.11 Nusselt number behavior for varying choices of ϕ and K	77

5.12 Nusselt number behavior for varying choices of ϕ and Nr	78
5.13 Nusselt number behavior for varying choices of Q and ϕ	78

List of Tables

3.1	Thermophysical characteristics of water-based copper nanoparticles. . .	32
4.1	Thermophysical characteristics of various nanoparticles and basefluid (water). [45].	49
4.2	Comparison of $-\theta'(1)$ for various mesh size when $M = 10$, $Pr = 6.2$, $\phi = 0.1$ and $Re = 7$	54
4.3	Comparison with results of $-\theta'(1)$ obtained by Ishak [36] and Wang [42] when $Pr = 7$, $\phi = 0$ and $Re = 1$	54
4.4	For various nanofluids, influence of Magnetic parameter on C_f , when $\phi = 0.1$, $Pr = 6.2$ and $Re = 1$	61
4.5	For various nanofluids, influence of M on Nu , when $Re = 1$, $Pr = 6.2$, and $\phi = 0.1$	61
4.6	For various nanofluids, influence of nanoparticle volume fraction on C_f , when $M = 5$, $Pr = 6.2$ and $Re = 1$	62
4.7	For various nanofluids, influence of Nanoparticle volume fraction on Nu , when $Pr = 6.2$, $Re = 1$, and $M = 5$	62
5.1	Thermophysical characteristics of various nanoparticles and basefluid [45].	65

5.2	Comparison of skin friction coefficient for various nanoparticles, when $\phi = 0.1$, $Pr = 6.2$, and $Re = 1$	69
5.3	Comparison of Nusselt number for various nanoparticles, when $Re = 1$, $Pr = 6.2$, and $\phi = 0.1$	69
5.4	Results of Nu and C_f for varying choices of ϕ , M, Nr, K and Q with $Re = 1$ and $Pr = 6.2$	79
6.1	Dimensions	90

Chapter 1

Introduction

Flow through a cylindrical shaped objects is of great importance at industrial scale as well as in our daily life challenges. For example, heart pumping and blood distribution in body through blood vessels, water distribution through cylindrical pipes, gas used for cooking purpose is also stored in cylindrical shaped cylinders. The main reason of using cylindrical shape duct is to minimize drag force effect on surface so that fluid can move easily. Pressure is applied in appropriate manners to control fluid movement. This phenomenon of flow movement under pressure is termed as pulsatile flow. Keeping the aforementioned in mind, numerous studies have been conducted for better understanding of pulsatile flow.

Nanofluids acquire a lot of attention due to their potential developments. Nanofluids are nanoparticles (< 100 nm in size) suspension in fluid that exhibit considerable enhancement properties even at low nanoparticle concentration. The most frequently used nanoparticles are metals (*Ag, Cu, Au*), oxides (*CuO, Al₂O₃, TiO₂, etc.*), carbon nanotubes, and carbides (*SiC*) whereas water, ethylene glycol, and oil are considered as base fluid. Choi [1] was the one who first came up with the idea of nanofluids and

use of these in a wide range of industries, including energy production, electronics, textiles, and paper manufacturing. Due to increased stability and thermal conductivity, nanofluids are extensively used as heat transfer media, even with small volume fractions of suspended nanoparticles. Suspended fluid particles are expected to have higher thermal conductivity as compare to ordinary fluids. Nanoparticle suspension in the fluid enhance heat transfer, effective thermal conductivity, viscosity and thermal diffusivity [2]. Heat transfer induced by fluid flow is a major research field of fluid mechanics. Therefore, in recent years, researchers have paid attention to heat transfer mechanism. Analysis of the heat transfer model is affected by many factors, such as volume fraction, flow geometry, boundary conditions and thermal characteristics of nanoparticles and base fluid characteristics. Buongiorno [3] introduced nanofluids heat transfer through a considerable slip mechanism. In the presence of a magnetic field, Akbar and Nadeem [4] studied a viscoelastic fluid model with mixed convection. Later on, researchers discussed and analyzed fluid flow phenomenon for various nanoparticles having different geometries [5-9].

Vardanyan [10] develops a variety of interesting analytical models to analyze the influence of magnetohydrodynamics (MHD) on flow through cylindrical ducts. Richardson and Tyler [11] confirmed the presence of maximum flow velocity near the nozzle. Atabek and Chang [12] presented the fundamental concepts and numerical solutions for the velocity profile for unsteady flow in a cylindrical duct. Sucec [13] analyzed the reaction characteristics of mean temperature and wall temperature across laminar fluid drift and horizontal flate plate. Due to pulsatile flow, oscillatory body acceleration effect on the blood movement is described by Chaturani and Palanisamy [14]. They use finite Hankel and Laplace transform to find analytical solution of pulsatile blood flow. As the diameter of tube grows, axial velocity causes fluid momentum to

be transferred from the tube's axis to the adjacent portion of the tube wall. Recently, Shahed [15] achieved the closed form solutions using Hankel and Laplace transforms for flow inside the porous channel with the pulsating blood flow. Furthermore, results are obtained in the form of Bessel-Fourier series by using Hankel and Laplace transform. Majdalani and Chibli [16] found the exact solution of Navier-Stokes equation, which determines pulsatile flow through a duct. The pressure gradient influence on velocity with phase difference is explored by Yakhot and Grinberg [17]. Under normal circumstances, Sanyal and Biswas [18] demonstrated that blood circulation in the human body is dependent on the coronary heart pumping blood. This phenomena takes place due to pressure gradient throughout the body.

In this thesis, review of [19] is presented which analyze the magneto-hydrodynamics flow of water oriented copper (Cu) nanoparticles between two concentric cylinders . Flow is induced by means of oscillatory pressure gradient. Cu nanoparticles have significant importance in the field of biomedicine, optics, nanofluids, and electronics. Cu nanoparticles are used to cure diseases such as thyroid glands, eradicate tumor, repair of tissues, reduce cholesterol, and help in the production of red blood cells. The fundamental governing equations are derived from basic momentum and heat equations, and then solved analytically to obtain exact solutions in the form of Bessel functions. The results acquired for temperature and velocity distribution and for pressure gradient are used to illustrate graphical results for various physical parameters. The pressure gradient is evaluated for various time intervals.

Research of magnetic field effects has attracted great attention due to its numerous applications in flow meters, pumps, liquid metal cooling systems, MHD generators, and metallurgy. The MHD basic concept is to induce current through a magnetic field in a moving conductive fluid, and the induced current tends to generate a force that

acts on ions in the conductive fluid. Initially, Bansal [20] introduced the concept of magnetohydrodynamics (MHD). The most frequent problem used in fluid mechanics in the presence of a transverse magnetic field is the hydromagnetic behavior of the boundary layer across static or moving surfaces. For incompressible fluid, Crane [21] examined the steady boundary layer flow. Existence of steady viscous flow across a stretching sheet explored by Miklavcic and Wang [22]. While working on the fluid flow across unsteady stretching sheet Wang [23] discussed flow across stretching sheet. Fang and Zhang [24] analyzed magnetic field influence on shrinking sheet flow and discussed how the strapping magnetic field maintains a constant steady state flow. Pavlov [25] studied the transverse magnetic field influence on the movement of a conductive liquid flowing across a stretching surface. Ishak et al. [26] examined the stagnation point two-dimensional MHD flow of stretched layers with different surface temperature, and revealed that at surface heat transfer tends to increase due to magnetic parameter. In a rectangular duct, magnetic field influence on the natural convection is analyzed by Rudraiah et al. [27], and revealed that magnetic field slows down the heat transfer rate. Kumaran et al. [28] examined the MHD boundary layer transition across a stretching sheet and found that as the magnetic parameter increases, skin friction coefficient and wall temperature decreases. Cooling and fluid heating is important for transportation and manufacturing. Different cooling strategies are designed for high energy systems. Owing to low thermal performance effects, fluids including ethylene glycol, engine oil and water have low heat transfer capacity. The conductive liquids can be suppressed or controlled by the body's electromagnetic force (Lorentz force). Interaction between electric current and applied magnetic field affects the Lorentz force. Fluid flow in a porous medium has been an area of intense research over the years. Natural convection with saturated porous material in a vertical annulus analyzed by

Parsad et al. [29]. Yih [30] examine the radiation influence on natural convection across vertical cylinder. Badruddin et al. [31] analyzed the viscous dissipation and radiation effect in annular porous channel. Butt et al. [32] determined the influence of MHD flow across stretching cylinder in a porous media, and observed that momentum boundary layer thickness depreciates for large magnetic parameter and permeability parameter. Thermal conductivity, heat source or sink, and dynamic viscosity influence on nanofluid in the presence of porous stretched tube is determined by Ahmed et al. [33]. Ishak et al. [34] analyzed suction/injection effect on steady, incompressible fluid across a permeable stretching tube, and proposed that skin friction coefficient escalates as Reynolds number grows.

The problem [35] is governed by non-linear differential equation of third order, which leads to an exact similarity solution of the momentum equation. For a conductive incompressible viscous fluid outside a stretching cylinder, flow and heat transfer in the presence of a transverse magnetic field is discussed by Ishak et al. [36]. Nonlinearity is inherent throughout many mathematical problems. It is crucial to devise effective strategies to resolve them. Despite the development of high-performance computers and computation tools, obtaining analytical approximation of non-linear partial differential equations is still a challenging task. To analyze convective flow of nanofluids, researchers formulated a variety of models and methods to solve complex geometries of multiple problems. In a semi-annulus enclosure filled with nanofluid, Sheikholeslami et al. [37] explored the natural convection heat transfer and revealed that inclination has a significant impact on the local Nusselt number maximum and minimum values, isotherms and streamlines. Sheikholeslami et al. [38] examined nanoparticles and magnetic field influence on the Jeffery-Hamel flow, and found that for increasing values of Hartmann number, backflow turns down. To reduce backflow at increasing angles or

Reynolds number, large values of Hartmann number are required. In addition, findings claimed that increasing values of nanoparticle volume fraction (ϕ) gives rise to the thickness of momentum boundary layer. Domairry et al. [39] analysis revealed that momentum boundary layer enlarges for greater volume fraction (ϕ), while reverse trend is observed for thermal boundary layer. In a horizontal cylindrical tube containing nanofluid, radial magnetic field influence on natural heat transfer convection is explored by Ashorynejad et al. [40]. Further, observations claimed that local Nusselt number will increase as the volume fraction and Rayleigh number increases, but due to strong magnetic field this effect diminishes.

The main purpose of present research is to analyze heat transfer and nanofluid flow in the presence of a magnetic field, across a stretched cylinder in a porous medium. Tiwari and Das [41] suggested nanofluid model for current problem [35]. Moreover, nanoparticle volume fraction (ϕ), thermal radiation (Nr), Reynolds number (Re), porosity parameter (K), rate of heat generation or absorption coefficient (Q), and magnetic parameter (M) influence on local Nusselt number and skin friction coefficient are discussed and analyzed. Water is used as a base fluid for copper nanoparticles. The MATLAB tool *bvp4c* is used to find similarity solutions. Numerical solution of reduced ordinary differential equations are evaluated using *bvp4c*. The velocity, temperature, and pressure distribution for various fluid parameters are analyzed graphically .

The overview of this thesis is given as:

Chapter 2 comprises of basic definitions of fluid flow, basic governing equations (continuity, momentum, energy) and heat transfer. Apart from these definitions, dimensionless quantities, thermophysical properties of nanofluids and all other necessary concepts are discussed in this chapter.

Chapter 3 is a review work of Shehzad et al. [19]. Mathematical model is es-

tablished for MHD flow of water-driven copper nanoparticles among two concentric cylinders. Closed form solutions are obtained in terms of Bessel functions. The effect of several parameters on pressure gradient, temperature and velocity profile is depicted graphically in the confined domain.

Chapter 4 is a review work of Ashorynejad [35], in which heat transfer of nanofluids in the existence of magnetic field through stretching cylinder is explored. Using similarity transformations, the governing partial differential equations convert to the set of ordinary differential equations with suitable boundary conditions. Compact solutions are obtained by using MATLAB package *bvp4c*. For various nanoparticles, graphical illustrations are presented for different parameters like Reynolds number, local Nusselt number, magnetic parameter, skin friction coefficient, and nanoparticle volume fraction.

Chapter 5 extends the mathematical model presented in Chapter 4 with effect of thermal radiation in a porous medium. Graphs and tabular results are obtained for several controlling parameters (such as magnetic parameter, porosity parameter, thermal radiation, nanoparticle volume fraction, heat absorption coefficient).

Chapter 6 sums up the concluding remarks of this dissertation.

Chapter 2

Preliminaries and basic concepts

This chapter contains specific concepts of fluid flow, specific equations with respect to fluid flow and heat transfer along with physical parameters of nanofluid.

2.1 Fluid and fluid flows

A fluid is a particular kind of matter that goes through steady distortion under applied pressure, substances that have ability to flow are termed as fluids. This includes liquids, gases, plasma's and some plastic solids. The phenomenon in which fluid continuously deforms itself is known as fluid flow.

2.2 Compressible and incompressible flows

A fluid flow in which the density variations are negligible is known as the incompressible flow. All liquids are considered as incompressible fluids. Contrarily, compressible fluids are fluids with variable density. Most commonly encountered gases are compressible.

Continuity equations for compressible and incompressible flows are respectively:

$$\frac{D\rho}{Dt} + \nabla \cdot (\rho \mathbf{V}) = 0, \quad (2.1)$$

$$\nabla \cdot \mathbf{V} = 0, \quad (2.2)$$

where ρ indicates fluid density, \mathbf{V} represents velocity vector and $\frac{D}{Dt}$ is material derivative which is given as:

$$\frac{D}{Dt} = \frac{\partial}{\partial t} + \nabla \cdot \mathbf{V}. \quad (2.3)$$

2.3 Laminar and turbulent flows

Laminar flow is the type of fluid flow in which fluid moves smoothly in parallel layers. The path lines of fluid flow do not cross each other. This flow usually occurs while dealing with low Reynolds number. The fluid flow in which fluid particles continuously changes their direction is known as turbulent flow. The flow is either turbulent or laminar is specified by Reynolds number.

2.4 Steady and unsteady flows

Flows in which properties of fluid at a particular point remains constant with time is known as steady flow. Mathematically steady flow is expressed as:

$$\frac{Du}{Dt} = 0, \quad (2.4)$$

In above equation t is time and u is any fluid property. Contrarily, flows in which fluid at particular point changes its properties with time is known as unsteady flow.

Mathematically, unsteady flow is expressed as:

$$\frac{Du}{Dt} \neq 0. \quad (2.5)$$

2.5 Pulsatile flow

Flow with periodic variations is known as pulsatile flow. Peristaltic motion of food in intestine, blood supply through an artery are examples of pulsatile flow.

2.6 Newtonian and non-Newtonian fluids

Newtonian fluids are specified as fluids that obey Newton's law of viscosity. Most common Newtonian fluids are air, water, sugar solution, organic solvents, gasoline, and glycerine etc. Non-newtonian fluids have the property that their shear stress is not linearly proportional to their deformation rate. Ketchup, jams, butter, blood, soap, yogurt, shampoo, honey, and toothpaste are few examples of non-newtonian fluids.

2.7 Axi-symmetric flow

A flow pattern is referred as axi-symmetric flow when it is identical in every plane that passes through certain straight line.

2.8 Viscosity

Viscosity is a quantity that shows fluid opposition to the deformation or shear stress and measured by the coefficient of viscosity (μ).

Mathematically:

$$\mu = \frac{\text{shear stress}}{\text{deformation rate}}. \quad (2.6)$$

In Eq.(2.6) μ is absolute or dynamic viscosity and it has S.I unit ($N.s/m^2$).

The other type of viscosity is termed as kinematic viscosity ν , which is the ratio of dynamic viscosity (μ) to density (ρ).

Mathematically:

$$\nu = \frac{\mu}{\rho}. \quad (2.7)$$

S.I unit of kinematic viscosity is (m^2/s). The fluids having non-zero viscosity are known as viscous fluids while those having zero dynamic viscosity are known as inviscid fluids.

2.9 Conservation laws

The analysis of a fluid dynamic problems usually involves the velocity field to describe flow pattern. The fluid in motion must satisfy the fundamental principles of mechanics (laws of mass, momentum and energy conservation) a constitutive relation and associated boundary conditions.

2.9.1 Continuity equation

From law of conservation of mass, continuity equation is derived. According to this law, amount of mass entering or leaving a fixed area (control volume) remains constant.

Mathematically:

$$\frac{D\rho}{Dt} + \nabla \cdot (\rho \mathbf{V}) = 0, \quad (2.8)$$

where \mathbf{V} represents velocity vector and ∇ is the differential operator. If ρ is constant, then for incompressible fluid Eq. (2.8) becomes

$$\nabla \cdot \mathbf{V} = 0. \quad (2.9)$$

2.9.2 Momentum equation

From Newton's second law of motion, momentum equation is derived. According to this law momentum in a system remains invariant until an external force is applied. It is also known as Navier-Stokes equation and can be expressed as:

$$\rho \frac{D\mathbf{V}}{Dt} = \nabla \cdot \boldsymbol{\tau} + \rho \mathbf{g}, \quad (2.10)$$

where $\rho \mathbf{g}$ denotes the body force in the system and $\boldsymbol{\tau}$ is Cauchy stress tensor.

$$\nabla \cdot \boldsymbol{\tau} = \mu \nabla^2 \mathbf{V} - \nabla p. \quad (2.11)$$

where p is pressure and $\nabla \cdot \boldsymbol{\tau}$ represent surface forces. Then Eq. (2.10) becomes:

$$\rho \frac{D\mathbf{V}}{Dt} = -\nabla P + \mu \nabla^2 \mathbf{V} + \rho \mathbf{g}. \quad (2.12)$$

.

2.9.3 Energy equation

From first law of thermodynamics, energy equation is derived. This law states that rate of work done owing to body or surface forces and rate of heat addition is equal to

rate of change of fluid energy within a control volume. It can be defined as:

$$\rho c_p \frac{DT}{Dt} = \nabla \cdot (\kappa \nabla \mathbf{T}) + f \cdot \mathbf{V}. \quad (2.13)$$

In Eq. (2.13) f is body or surface force, c_p denotes specific heat at a constant temperature, and κ is thermal conductivity of the fluid,.

2.10 Porous medium

A porous medium or porous material is a substance composed of persistent solid particles (solid matrix) and the remaining void space can be filled with one or more fluids such as oil, gas, and water. Foam cemented sandstone, sand, bread, and soil are examples of porous medium.

2.11 Vortex

A region in a fluid in which flow revolves around an axis line is known as vortex (vortices). It may be curve or straight, whirlpool and tornado are examples of vortex flow. Vortex is curl of velocity field. Mostly, vortices have maximum fluid velocity along their axis.

2.12 Boundary conditions

Boundary conditions are defined as a set of conditions that must be satisfied in a region where the system of differential equations acquire to be solved.

2.12.1 Slip condition

The phenomenon in which fluid velocity at surface is proportional to shear stress present at surface is termed as slip boundary condition.

2.12.2 No-slip condition

In this phenomenon fluid flowing over a solid surface has zero velocity relative to boundary.

2.13 Magnetohydrodynamics

Magnetohydrodynamics (MHD) is a branch of engineering that investigates the behavior of magnetic field in electrically conducting fields. The set of equations that identifies MHD flow is obtained by combining Maxwell's equation and equations of motion. The momentum Eq.(2.10) with electromagnetic force for MHD fluid flow is

$$\rho \frac{D\mathbf{V}}{Dt} = \nabla \cdot \boldsymbol{\tau} + (\mathbf{J} \times \mathbf{B}), \quad (2.14)$$

where \mathbf{J} is the current density, \mathbf{B} is total magnetic field and has a following expression:

$$\mathbf{B} = \mathbf{B}_o + \mathbf{B}_i, \quad (2.15)$$

where \mathbf{B}_i is the induced magnetic field and \mathbf{B}_i is assumed to be very small thus it can be neglected when compared with external magnetic field. This is justified for MHD

flow with small Reynolds number. According to Ohm's law, \mathbf{J} is stated as:

$$\mathbf{J} = \sigma(\mathbf{E} + \mathbf{V} \times \mathbf{B}). \quad (2.16)$$

The electrical field \mathbf{E} is assumed to be zero and σ is electrical conductivity. After simplification

$$\mathbf{J} \times \mathbf{B} = \sigma(\mathbf{V} \times \mathbf{B}) \times \mathbf{B}. \quad (2.17)$$

as $\mathbf{B} = \mathbf{B}_o$, since induced magnetic field is neglected. Using Eq. (2.17), momentum Eq. (2.14) becomes:

$$\rho \frac{D\mathbf{V}}{Dt} = \nabla \cdot \boldsymbol{\tau} - \sigma B_o^2 \mathbf{V}. \quad (2.18)$$

2.14 Heat transfer mechanism

Heat transfer takes place among two bodies with distinct temperature. Heat moves from high to low temperature (warm body to cold one) until the equilibrium is achieved. The heat transfer process occurs by convection, radiation, and conduction.

2.14.1 Convection

In this process, heat transfer takes place by movement of particles in liquid. Within the process energy transfer takes place from a higher temperature region to lower temperature region. Mathematically form is expressed as:

$$Q = hA(T - T_\infty), \quad (2.19)$$

where Q is heat transferred per unit time, h is coefficient of convection, A is cross-sectional area, T is temperature and T_∞ is temperature outside the environment.

2.14.2 Radiation

Radiation occurs by photons of light or waves emitted from a surface volume. Radiation can also occur in vacuum. Stefan-Boltzmann law is used to calculate the amount of heat transfer through radiation. Mathematically:

$$Q = \sigma^* \cdot T^4, \quad (2.20)$$

where, σ^* denotes Stefan-Boltzmann's constant and T is temperature.

2.14.3 Conduction

Transfer of heat by interaction of molecules from one substance to another is known as conduction. Mostly conduction occurs in solids. Fourier developed a law known as Fourier's law of heat conduction. Mathematically:

$$Q = -\kappa A \frac{dT}{dx} \quad (2.21)$$

where Q is heat transferred per unit time, A is cross-sectional area, κ is thermal conductivity, and $\frac{dT}{dx}$ is temperature gradient.

2.15 Boundary layer

The layer of fluid over the surface where viscosity effects are significant is called a boundary layer. Viscosity is maximum near surface and it decreases gradually as fluid moves away from surface.

2.16 Skin friction coefficient

Measure of resistance between the solid surface and fluid is known as skin friction coefficient. It is defined as:

$$C_f = \frac{\tau_w}{\rho_f W_w^2}, \quad (2.22)$$

where τ_w is total wall shear stress and it is expressed as:

$$\tau_w = \mu_{nf} \left. \frac{\partial w}{\partial r} \right|_{r=a}. \quad (2.23)$$

2.17 Dimensionless parameters

Some well-known dimensionless parameters in fluid dynamics are mentioned below:

2.17.1 Reynolds number

The dimensionless parameter Re determines the ratio of inertial and viscous forces. It allows us to differentiate whether the flow is turbulent or laminar. High Reynolds number suggest turbulent behavior due to dominant inertial forces. Whereas, laminar behavior is observed at low Reynolds number which shows that viscous forces are dominant.

Mathematical expression is written as:

$$Re = \frac{\text{inertial force}}{\text{viscous force}} = \frac{vL}{\nu}, \quad (2.24)$$

where L is characteristic length of fluid, v is velocity, and ν is the kinematic viscosity of fluid.

2.17.2 Nusselt number

It appears when there is a heat transfer from convection flow to conduction flow in fluids across boundary. The heat transfer is perpendicular to the surface of boundary.

Mathematically:

$$Nu = \frac{Q}{\frac{\kappa}{L}} = \frac{QL}{\kappa}, \quad (2.25)$$

where κ is the thermal conductivity of fluid, Q represents convective heat transfer, and L denotes characteristic length.

2.17.3 Hartmann number

The ratio of electromagnetic forces and viscous forces is known as Hartmann number, which mainly exists in the fluid flowing through a magnetic field.

Mathematically:

$$Ha = \frac{\text{electromagnetic force}}{\text{viscous force}} = BL\sqrt{\frac{\sigma}{\mu}}, \quad (2.26)$$

where B denotes magnetic field, σ is electrical conductivity, μ is dynamic viscosity of nanofluid, and L is characteristic length.

2.17.4 Prandtl number

The dimensionless parameter quantifies the ratio of momentum diffusivity (ν) and thermal diffusivity (α), and it is used to characterize relative thickness of momentum and thermal boundary layer.

Mathematically:

$$Pr = \frac{\text{Momentum diffusivity}}{\text{Thermal diffusivity}} = \frac{\nu}{\alpha} \quad (2.27)$$

2.18 Nanofluids

Nanofluids are special kind of fluids that have improved thermal conductivity. Nanofluids include base fluid (water, oil, ethynol, etc.) in which particles of a nano-meter-sized scale (1-100 nm) are suspended. Metals (*Cu, Ag*), oxides (*Al₂O₃, CuO, TiO₂*) forms several common nanoparticles used to create nanofluids.

2.19 Thermophysical properties of nanofluid

Following are some thermophysical properties of nanofluids.

2.19.1 Specific Heat

It is amount of energy which require to increase temperature by one degree Celcius per unit mass. It is denoted by c_p and S.I unit is (J/(K.kg)).

Mathematical expression is given by Faisal et al. [19] as:

$$(\rho c)_{nf} = (1 - \phi) (\rho c)_f + \phi (\rho c)_p, \quad (2.28)$$

where c_p is nanoparticle specific heat and c_f is basefluid specific heat capacity.

2.19.2 Density

Amount of mass per unit volume is called density. It is denoted by ρ and S.I unit is (kg/m^3).

Density of nanofluid given by Faisal et al. [19] has following expression :

$$\rho_{nf} = (1 - \phi) \rho_f + \phi \rho_p, \quad (2.29)$$

where ρ_p is nanoparticles density and ρ_f is density of base fluid.

2.19.3 Dynamic viscosity

Dynamic viscosity is measure of fluid's viscosity, it determines how dense the fluid is.

The S.I unit is ($kg/m.s$) and viscosity of nanofluid given by Faisal et al. [19] as:

$$\mu_{nf} = \frac{\mu_f}{(1 - \phi)^{2.5}}, \quad (2.30)$$

where μ_f is dynamic viscosity of base fluid, and ϕ is nanoparticle volume fraction.

2.19.4 Thermal conductivity

Thermal conductivity is defined as materials ability to conduct or transfer heat. It is denoted by κ and its S.I unit is ($W/(m.K)$).

Mathematical expression of thermal conductivity given by Faisal et al. [19] is as follows:

$$\kappa_{nf} = \kappa_f \left[\frac{\kappa_p + 2\kappa_f - 2\phi(\kappa_f - \kappa_p)}{\kappa_p + 2\kappa_f + \phi(\kappa_f - \kappa_p)} \right], \quad (2.31)$$

where κ_p is thermal conductivity of nanoparticle, κ_{nf} denotes thermal conductivity of nanofluids, κ_f is thermal conductivity of the base fluid.

2.19.5 Electrical conductivity

It is defined as a measure of materials capacity to hold electric current or amount of current it can bear. The S.I unit is (S/m) .

Mathematical expression of electrical conductivity given by Faisal et al. [19] as:

$$\frac{\sigma_{nf}}{\sigma_f} = 1 + \frac{3 \left(\frac{\sigma_p}{\sigma_f} - 1 \right) \phi}{\left(\frac{\sigma_p}{\sigma_f} + 2 \right) - \left(\frac{\sigma_p}{\sigma_f} - 1 \right) \phi}, \quad (2.32)$$

where σ_p denotes electrical conductivity of nanoparticles and σ_f denotes electrical conductivity of the fluid.

Chapter 3

Water driven copper nanoparticles between two concentric cylinders with an oscillatory pressure gradient

This chapter covers the review of [19]. In the presence of copper nanoparticles, the unidirectional MHD flow of viscous fluid with heat transmission is discussed. Constitutive equations of conservation of mass, energy, and momentum are based upon partial differential equations which contains thermophysical characteristics for both base fluid and nanoparticles. Mathematical formulation of flow and heat transfer model, as well as pressure calculations along with graphical illustrations are discussed in this chapter.

3.1 Problem formulation

Assume the unidirectional MHD flow of viscous, electrically conducting, incompressible fluid moving among two concentric cylinders. Nanoparticles are added to the base fluid

to improve its thermal conductivity. In the z -direction, pulsatile pressure gradient is introduced to move the fluid within the specified channel. The magnetic field B_o is taken along r -direction. As the fluid flows due to the pulsatile pressure, velocity at walls of cylinder becomes zero. However, external duct temperature is adiabatic and temperature of internal duct is uniform (400 Kelvin). Moreover, atmospheric pressure and temperature are considered to be around 300 Kelvin, with $\vec{V}=V(u, v, w)$ representing velocity field. The geometry of problem is given by [19] in Figure 3.1.

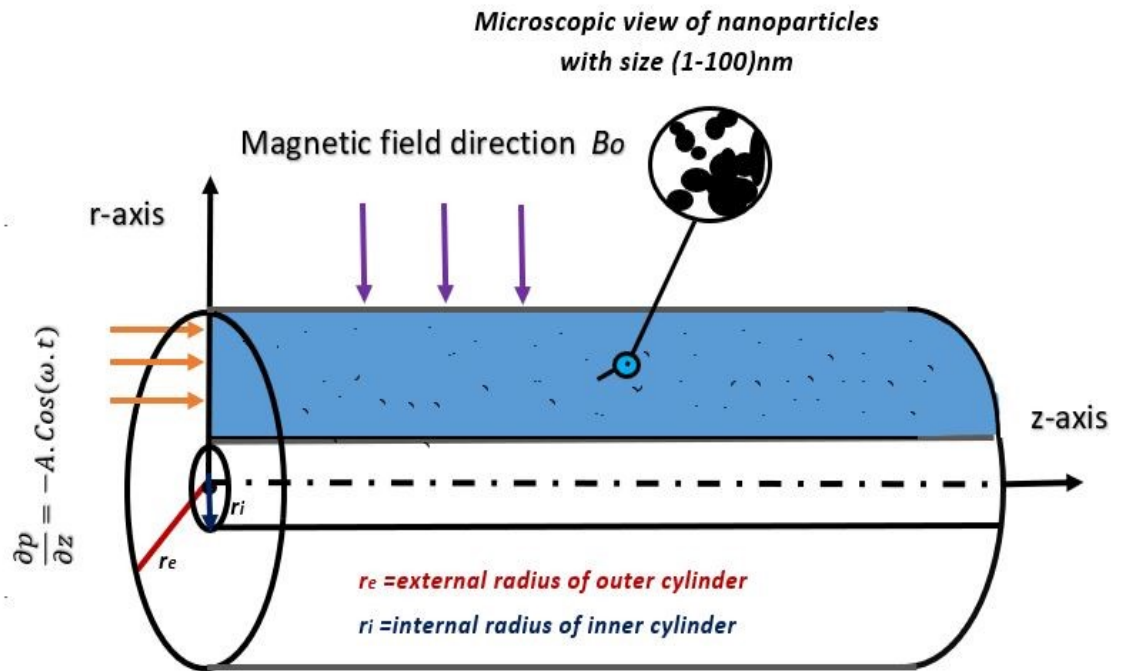


Figure 3.1: Flow field geometry.

Accounting these assumptions, the constitutive equations that describe the fluid flow between concentric cylinders are:

$$\nabla \cdot \vec{V} = 0, \quad (3.1)$$

$$\rho_{nf} \left[\frac{\partial \vec{V}}{\partial t} + (\vec{V} \cdot \nabla) \vec{V} \right] = -\nabla p + \mu_{nf} \nabla^2 \vec{V} + (\vec{J} \times \vec{B}), \quad (3.2)$$

$$(\rho c)_{nf} \left[\frac{\partial T}{\partial t} + (\vec{V} \cdot \nabla) T \right] = \kappa_{nf} \nabla^2 T. \quad (3.3)$$

In cylindrical coordinate system, Eqs. (3.1)-(3.3) becomes:

$$\frac{\partial u}{\partial r} + \frac{\partial w}{\partial z} + \frac{u}{r} = 0, \quad (3.4)$$

$$\rho_{nf} \left[\frac{\partial u}{\partial t} + u \frac{\partial u}{\partial r} + w \frac{\partial u}{\partial z} \right] = -\frac{\partial p}{\partial r} + \mu_{nf} \left[\frac{\partial^2 u}{\partial r^2} + \frac{1}{r} \frac{\partial u}{\partial r} - \frac{u}{r^2} + \frac{\partial^2 u}{\partial z^2} \right], \quad (3.5)$$

$$\rho_{nf} \left[\frac{\partial w}{\partial t} + u \frac{\partial w}{\partial r} + w \frac{\partial w}{\partial z} \right] = -\frac{\partial p}{\partial z} + \mu_{nf} \left[\frac{\partial^2 w}{\partial r^2} + \frac{1}{r} \frac{\partial w}{\partial r} + \frac{\partial^2 w}{\partial z^2} \right] - \sigma_{nf} B_o^2 w, \quad (3.6)$$

$$(\rho c)_{nf} \left[\frac{\partial T}{\partial t} + u \frac{\partial T}{\partial r} + w \frac{\partial T}{\partial z} \right] = \kappa_{nf} \left[\frac{\partial^2 T}{\partial r^2} + \frac{1}{r} \frac{\partial T}{\partial r} + \frac{\partial^2 T}{\partial z^2} \right], \quad (3.7)$$

where T is temperature and p is pressure. Mathematical expression of nanofluid properties such as, dynamic viscosity (μ_{nf}), electrical conductivity (σ_{nf}), density (ρ_{nf}), thermal conductivity (κ_{nf}), and specific heat ($(\rho c)_{nf}$) are expressed in Eqs. (2.28)-(2.32). In Eq. (3.6) ($-\sigma_{nf} B_o^2 w$) is derived from Eq. (2.17). In view of above mentioned parameters, Eqs. (3.5)-(3.7) will takes the following form:

$$\begin{aligned} & \rho_f \left[(1 - \phi) + \left(\frac{\rho_p}{\rho_f} \right) \phi \right] \left[\frac{\partial u}{\partial t} + u \frac{\partial u}{\partial r} + w \frac{\partial u}{\partial z} \right] \\ &= -\frac{\partial p}{\partial r} + \frac{\mu_f}{(1 - \phi)^{2.5}} \left[\frac{\partial^2 u}{\partial r^2} + \frac{1}{r} \frac{\partial u}{\partial r} - \frac{u}{r^2} + \frac{\partial^2 u}{\partial z^2} \right], \end{aligned} \quad (3.8)$$

$$\begin{aligned} & \rho_f \left[(1 - \phi) + \left(\frac{\rho_p}{\rho_f} \right) \phi \right] \left[\frac{\partial w}{\partial t} + u \frac{\partial w}{\partial r} + w \frac{\partial w}{\partial z} \right] \\ &= -\frac{\partial p}{\partial z} + \frac{\mu_f}{(1 - \phi)^{2.5}} \left[\frac{\partial^2 w}{\partial r^2} + \frac{1}{r} \frac{\partial w}{\partial r} + \frac{\partial^2 w}{\partial z^2} \right] - \sigma_{nf} B_o^2 w, \end{aligned} \quad (3.9)$$

$$\begin{aligned} & (\rho c)_f \left[(1 - \phi) + \left(\frac{(\rho c)_p}{(\rho c)_f} \right) \phi \right] \left[\frac{\partial T}{\partial t} + u \frac{\partial T}{\partial r} + w \frac{\partial T}{\partial z} \right] \\ &= \kappa_{nf} \left[\frac{\partial^2 T}{\partial r^2} + \frac{1}{r} \frac{\partial T}{\partial r} + \frac{\partial^2 T}{\partial z^2} \right]. \end{aligned} \quad (3.10)$$

For this model, corresponding initial and boundary conditions are:

When $t = 0$,

$$u(r, z, 0) = w(r, z, 0) = 0, \quad \text{and} \quad p(r, z, 0) = T_f(r, z, 0) = 0. \quad (3.11)$$

At outer cylinder,

$$u(1, z, t) = w(1, z, t) = 0, \quad \text{and} \quad \frac{\partial T_f}{\partial r}(1, z, t) = 0. \quad (3.12)$$

At inner cylinder,

$$u\left(\frac{r_i}{r_e}, z, t\right) = w\left(\frac{r_i}{r_e}, z, t\right) = 0, \quad \text{and} \quad T_f\left(\frac{r_i}{r_e}, z, t\right) = 1, \quad (3.13)$$

where r_i and r_e are internal radius of inner cylinder and external radius of outer cylinder respectively. To non-dimensionlize the Eqs. (3.8)-(3.10) subject to initial boundary

conditions Eqs. (3.11)-(3.13), the following set of dimensionless variables are introduced as:

$$\begin{aligned} u &= \frac{u'}{\omega r_e}, & w &= \frac{w'}{\omega r_e}, & r &= \frac{r'}{r_e}, & z &= \frac{z'}{r_e}, \\ t &= \omega t', & p &= \frac{p'}{r_e^2 \omega^2 \rho_f}, & T &= \frac{T' - T_f}{T_i - T_f}, & \nu_f &= \frac{\mu_f}{\rho_f}. \end{aligned} \quad (3.14)$$

Now we transform the above dimensional flow Eqs. (3.8)-(3.10) into non-dimensional form using Eq. (3.14).

$$A_1 \left[\frac{\partial u}{\partial t} + u \frac{\partial u}{\partial r} + w \frac{\partial u}{\partial z} \right] = -\frac{\partial p}{\partial r} + \frac{1}{(1-\phi)^{2.5} \text{Re}} \left[\frac{\partial^2 u}{\partial r^2} + \frac{1}{r} \frac{\partial u}{\partial r} + \frac{\partial^2 u}{\partial z^2} - \frac{u}{r^2} \right], \quad (3.15)$$

$$A_1 \left[\frac{\partial w}{\partial t} + u \frac{\partial w}{\partial r} + w \frac{\partial w}{\partial z} \right] = -\frac{\partial p}{\partial z} + \frac{1}{(1-\phi)^{2.5} \text{Re}} \left[\frac{\partial^2 w}{\partial r^2} + \frac{1}{r} \frac{\partial w}{\partial r} + \frac{\partial^2 w}{\partial z^2} \right] - \frac{A_2 M^2}{\text{Re}} w, \quad (3.16)$$

$$A_3 \left[\frac{\partial T}{\partial t} + u \frac{\partial T}{\partial r} + w \frac{\partial T}{\partial z} \right] = \frac{A_4}{\text{Pr.Re}} \left[\frac{\partial^2 T}{\partial r^2} + \frac{1}{r} \frac{\partial T}{\partial r} + \frac{\partial^2 T}{\partial z^2} \right]. \quad (3.17)$$

Non-dimensional boundary conditions are:

$$w = 0, \quad \frac{\partial T}{\partial r} = 0 \quad \text{at } r = 1 \quad (3.18)$$

$$w = 0, \quad T = 1 \quad \text{at } r = \frac{r_i}{r_e} = R^* \quad (3.19)$$

The dimensionless parameters appearing in partial differential Equations (3.15)-(3.17) are defined as:

$$\text{Pr} = \frac{\mu_f c_f}{\kappa_f}, \quad M = r_e B_o \sqrt{\frac{\sigma_f}{\mu_f}}, \quad \text{Re} = \alpha^2 = \frac{\omega r_e^2}{\nu_f}, \quad (3.20)$$

where Re is Reynolds number, α is Womersley number(= $\sqrt{\text{Re}}$), M is Hartmann

number, and Pr is Prandtl number. Coefficients A_1 , A_2 , A_3 , A_4 and A_5 are expressed as:

$$A_1 = (1 - \phi) + \left(\frac{\rho_p}{\rho_f} \right) \phi, \quad (3.21)$$

$$A_2 = \frac{\sigma_{nf}}{\sigma_f} = 1 + \frac{3 \left(\frac{\sigma_p}{\sigma_f} - 1 \right) \phi}{\left(\frac{\sigma_p}{\sigma_f} + 2 \right) - \left(\frac{\sigma_p}{\sigma_f} - 1 \right) \phi}, \quad (3.22)$$

$$A_3 = (1 - \phi) + \left(\frac{(\rho c)_p}{(\rho c)_f} \right) \phi, \quad (3.23)$$

$$A_4 = \frac{\kappa_{nf}}{\kappa_f} = \frac{\kappa_p + 2\kappa_f - 2\phi(\kappa_f - \kappa_p)}{\kappa_p + 2\kappa_f + \phi(\kappa_f - \kappa_p)}, \quad (3.24)$$

$$A_5 = \frac{1}{(1 - \phi)^{2.5}}. \quad (3.25)$$

Velocity field for the fully developed flow is considered as:

$$\vec{V} = [0, 0, w(r, z, t)]. \quad (3.26)$$

Fluid flow defined in Eq. (3.26) identically satisfies the continuity Eq. (2.9) and the Eqs. (3.15)-(3.17) can be rewritten as:

$$A_1 \frac{\partial w}{\partial t} = -\frac{\partial p}{\partial z} + \frac{A_5}{\text{Re}} \left[\frac{\partial^2 w}{\partial r^2} + \frac{1}{r} \frac{\partial w}{\partial r} \right] - \frac{A_2 M^2}{\text{Re}} w, \quad (3.27)$$

$$A_3 \left[\frac{\partial T}{\partial t} + w \frac{\partial T}{\partial z} \right] = \frac{A_4}{\text{Re.Pr}} \left[\frac{\partial^2 T}{\partial r^2} + \frac{1}{r} \frac{\partial T}{\partial r} + \frac{\partial^2 T}{\partial z^2} \right]. \quad (3.28)$$

3.2 Solution of the problem

The periodic pressure gradient, for the pulsatile flow is stated as follows:

$$\frac{\partial p}{\partial z} = -A \cos(\omega t) = \text{Real}(-Ae^{i\omega t}). \quad (3.29)$$

The velocity profile solution is expressed as:

$$W(r, t) = w(r, t) = \text{Real} [f(r)e^{it}]. \quad (3.30)$$

In the view of above Eqs. (3.29) and (3.30), Eq. (3.27) will takes the following form:

$$\frac{d^2 f(r)}{dr^2} + \frac{1}{r} \frac{df(r)}{dr} - \frac{1}{A_5} (A_2 M^2 + i\alpha^2 A_1) f(r) = -\frac{A\alpha^2}{A_5}. \quad (3.31)$$

The solution to linear second order ordinary differential equation (3.31) is in the form of Bessel functions,

$$f(r) = C_1 I_0(\beta r) + C_2 K_0(\beta r) + \frac{A\alpha^2}{\beta^2 A_5}, \quad (3.32)$$

where I_o and K_o are zeroth order modified Bessel functions of 1st and 2nd kind respectively, and $\beta = \sqrt{\frac{1}{A_5} (A_2 M^2 + i\alpha^2 A_1)}$.

Eq. (3.30) together with Eq. (3.32) yields,

$$w(r, t) = \text{Real} \left[C_1 I_0(\beta r) + C_2 K_0(\beta r) + \frac{A\alpha^2}{\beta^2 A_5} \right] e^{it}. \quad (3.33)$$

To determine the constants C_1 and C_2 Eqs. (3.18)-(3.19) are substituted in Eq. (3.33).

After simplification we get,

$$C_1 = -\frac{\alpha^2 BesselK[0, \beta]A - \alpha^2 BesselK[0, \beta R^*]A}{\beta^2 A_5 (BesselI[0, \beta R^*]BesselK[0, \beta] - BesselI[0, \beta]BesselK[0, \beta R^*])}, \quad (3.34)$$

$$C_2 = -\frac{-\alpha^2 BesselI[0, \beta]A + \alpha^2 BesselI[0, \beta R^*]A}{\beta^2 A_5 (BesselI[0, \beta R^*]BesselK[0, \beta] - BesselI[0, \beta]BesselK[0, \beta R^*])}. \quad (3.35)$$

To evaluate analytical solution of the Eq. (3.28), the temperature profile solution is assumed to be as follows:

$$T(r, z, t) = \text{Real} \left[-\gamma' .z + \gamma' .g(r).e^{it} + 1 \right], \quad (3.36)$$

where $\gamma' = \frac{r_c}{L}$. Equation (3.28) together with equation (3.36) is expressed as:

$$\frac{d^2 g(r)}{dr^2} + \frac{1}{r} \frac{dg(r)}{dr} - i \frac{A_3 Pr \alpha^2}{A_4} g(r) = \frac{A_3 Pr \alpha^2}{A_4} f(r). \quad (3.37)$$

Temperature profile solution will takes the following form:

$$T(r, z, t) = \text{Real} \left[-\gamma' .z + \gamma' [-iC_1 I_0(\beta r) - iC_2 K_0(\beta r) + C_3 I_0(\eta r) + C_4 K_0(\eta r) - i \frac{A\alpha^2}{\beta^2 A_5}] e^{it} + 1 \right], \quad (3.38)$$

where $\eta = \sqrt{i \frac{A_3 Pr \alpha^2}{A_4}}$. To determine the constants C_3 and C_4 use of Eqs. (3.18)-(3.19) in Eq. (3.38) gives

$$C_3 = \frac{\alpha \beta^2 A_5 \sqrt{i Pr A_3} BesselK[1, \eta] \zeta_1 + \beta^3 A_5 \sqrt{A_4} BesselK[1, \eta R^*] \zeta_2}{\alpha \beta^2 \sqrt{i Pr} (BesselK[1, \eta R^*] BesselI[1, \eta] + BesselK[1, \eta] BesselI[1, \eta R^*])}, \quad (3.39)$$

$$C_4 = \frac{\alpha \beta^2 A_5 \sqrt{i Pr A_3} BesselI[1, \eta] \zeta_1 - \beta^3 A_5 \sqrt{A_4} BesselI[1, \eta R^*] \zeta_2}{\alpha \beta^2 \sqrt{i Pr} (BesselK[1, \eta R^*] BesselI[1, \eta] + BesselK[1, \eta] BesselI[1, \eta R^*])}, \quad (3.40)$$

where,

$$\zeta_1 = i \left[C_1 I_0(\beta R^*) + C_2 K_0(\beta R^*) - i \frac{z}{e^{it}} + \frac{A \alpha^2}{\beta^2 A_5} \right], \quad (3.41)$$

$$\zeta_2 = i [C_1 I_1(\beta) - C_2 K_1(\beta)]. \quad (3.42)$$

3.2.1 Pressure

To compute the pressure gradient, Eq. (3.27) can be written as:

$$\frac{\partial p}{\partial z} = -A_1 \frac{\partial w}{\partial t} + \frac{A_5}{\alpha^2} \left[\frac{\partial^2 w}{\partial r^2} + \frac{1}{r} \frac{\partial w}{\partial r} \right] - \frac{A_2 M^2}{\alpha^2} w. \quad (3.43)$$

Eq. (3.43) together with Eq. (3.33) becomes:

$$\begin{aligned} \frac{\partial p}{\partial z} = & -A_1 \left[i.e^{it} \left(C_1 I_0(\beta r) + C_2 K_0(\beta r) + \frac{A\alpha^2}{\beta^2 A_5} \right) \right] \\ & + \frac{A_5}{\alpha^2} \left[e^{it} \left(\frac{\beta^2(I_2(\beta r) + I_0(\beta r))}{2} C_1 - \frac{\beta^2(K_2(\beta r) + K_0(\beta r))}{2} C_2 \right) \right] \\ & + \frac{A_5}{\alpha^2} \frac{e^{it}}{r} [\beta I_1(\beta r) C_1 - \beta K_1(\beta r) C_2] - \frac{A_2 M^2}{\alpha^2} \left[e^{it} \left(C_1 I_0(\beta r) + C_2 K_0(\beta r) + \frac{A\alpha^2}{\beta^2 A_5} \right) \right]. \end{aligned}$$

The non-dimensional pressure gradient is expressed as:

$$\Delta p = \int_0^1 \frac{\partial p}{\partial z} dz. \quad (3.44)$$

After simplification Eq. (3.44) becomes:

$$\begin{aligned} \Delta p = & -A_1 \left[i.e^{it} \left(C_1 I_0(\beta r) + C_2 K_0(\beta r) + \frac{A\alpha^2}{\beta^2 A_5} \right) \right] \\ & + \frac{A_5}{\alpha^2} \left[e^{it} \left(\frac{\beta^2(I_2(\beta r) + I_0(\beta r))}{2} C_1 - \frac{\beta^2(K_2(\beta r) + K_0(\beta r))}{2} C_2 \right) \right] \\ & + \frac{A_5}{\alpha^2} \frac{e^{it}}{r} [\beta I_1(\beta r) C_1 - \beta K_1(\beta r) C_2] - \frac{A_2 M^2}{\alpha^2} \left[e^{it} \left(C_1 I_0(\beta r) + C_2 K_0(\beta r) + \frac{A\alpha^2}{\beta^2 A_5} \right) \right]. \end{aligned}$$

In the next section graphical behavior under different parameters is analyzed.

3.3 Graphical analysis

The behavior of velocity and temperature distribution, vorticity, and pressure gradient for different controlling parameters (such as Prandtl number (Pr), nanoparticle volume fraction (ϕ), pressure gradient amplitude (A), Hartmann number (M), Reynolds number (Re), and time (t)) are discussed in separate subsections. These quantities are discussed for Cu as a nanoparticle. The thermophysical characteristics of nanofluids

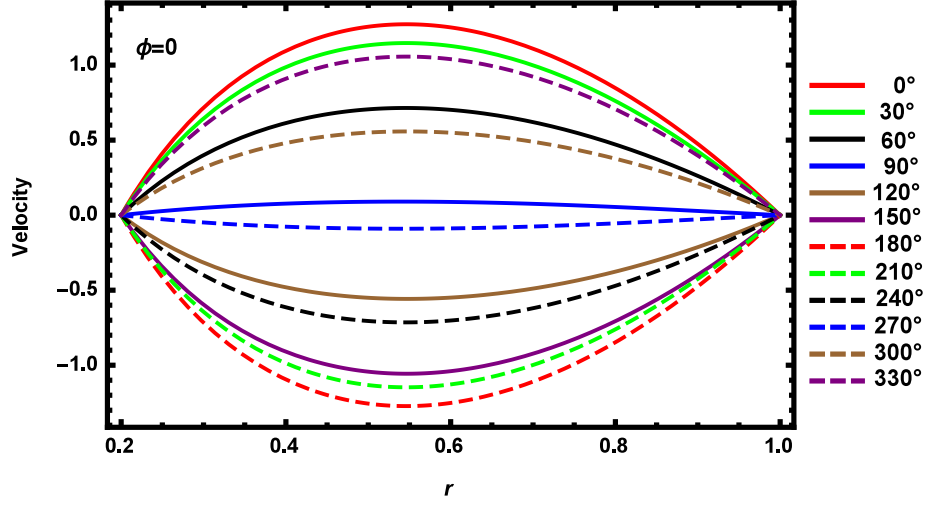
are listed below.

Table 3.1: Thermophysical characteristics of water-based copper nanoparticles.

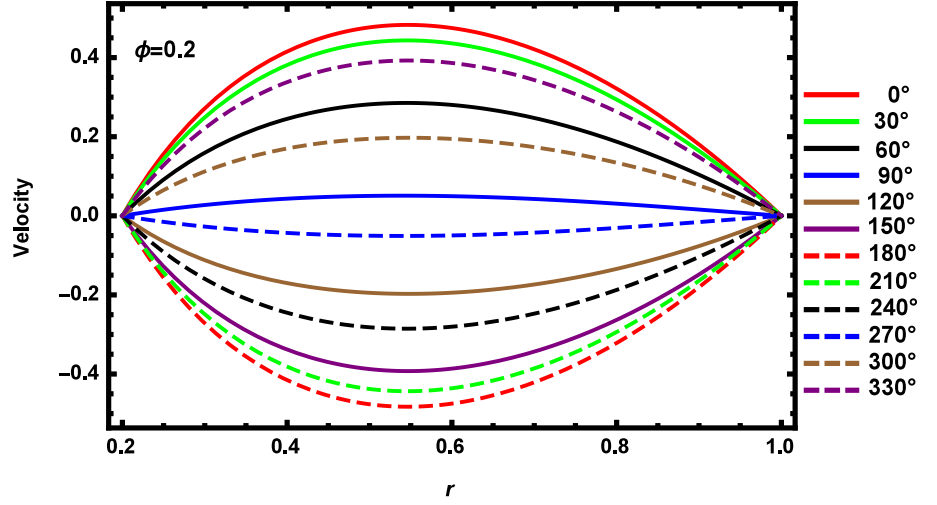
Phase	$\rho(Kg/m^3)$	$k(W/mK)$	$C(J/kgK)$	$\sigma(s/m)$
H_2O	997.1	0.613	4179	0.05
Cu	8933	400	385	5.96×10^7

3.3.1 Velocity

The effect of flow development on axial velocity is discussed. For a certain range, the rate of heat transfer and axial velocity changes from inlet to outlet. The velocity variance in axial direction against specified volume fraction (ϕ) is determined for one complete pulsation period of 360° . There are total of 12 instances for a complete cycle of 360° . In all the figures to follow values of parameter t are taken such that $0^\circ \leq t \leq 360^\circ$. In Figs. 3.2(a)-(b) velocity behavior against volume fraction (ϕ) is observed. Velocity profile follows a parabolic path. Velocity distribution will be highest at the channel's mean position and decreases rapidly for increasing values of ϕ . The density of whole mixture is increased when nanoparticles are added as shown in Figs 3.2(a)-(b). For base fluid ($\phi = 0$), velocity profile has a large and higher disturbance as shown in Fig 3.2(a). Physically, we assume that inclusion of nanoparticles into water raises the density of whole mixture significantly. When the density of nanofluids increases, the nanofluids motion becomes slower in comparison to base fluid, as observed in Fig 3.2(b).



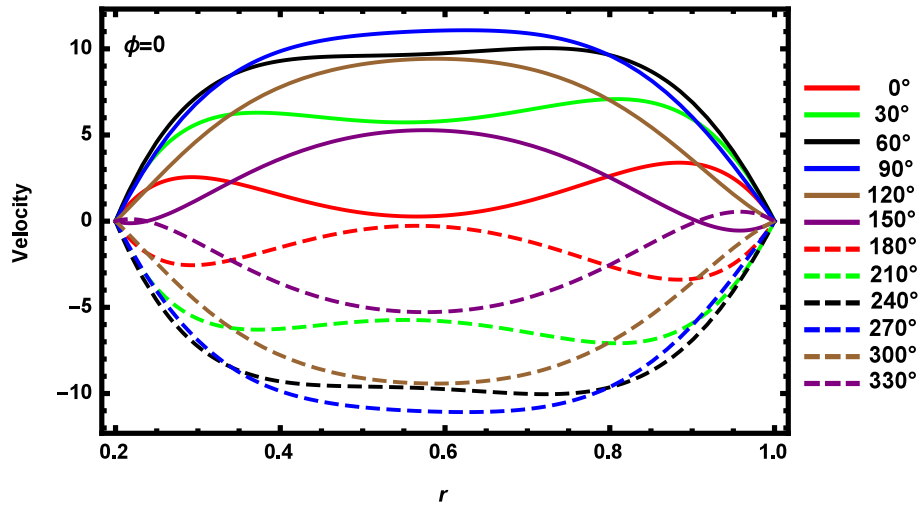
(a)



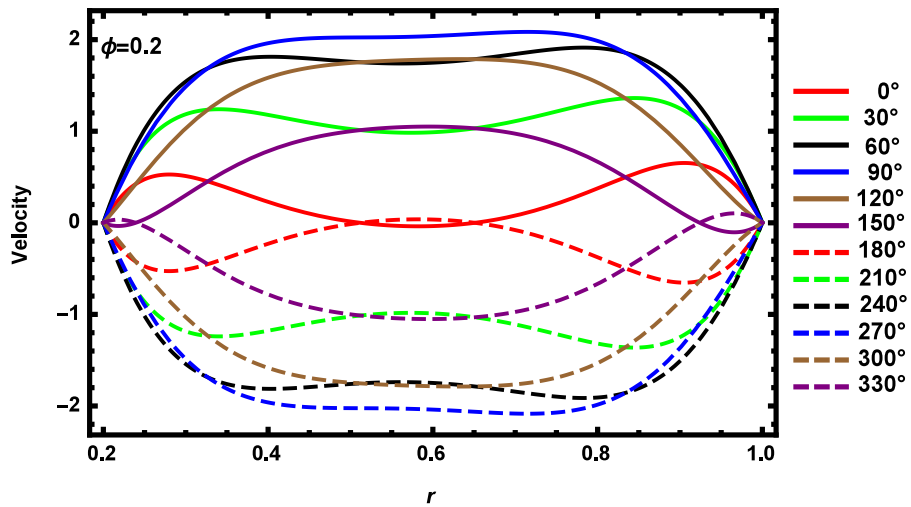
(b)

Figure 3.2: Velocity profile variance for $0^\circ \leq t \leq 360^\circ$ when $Re = 1$ and $M = 0$.

Figure 3.3(a)-(b) shows that due to annular effect, maximum velocity is located near cylinder walls with rapid vibrations. Reynolds number tends to rise annular effects. Further, it is noticed that radial velocity near cylinder wall becomes steeper as the Reynolds number (Re) increases and as a result frictional forces increase.



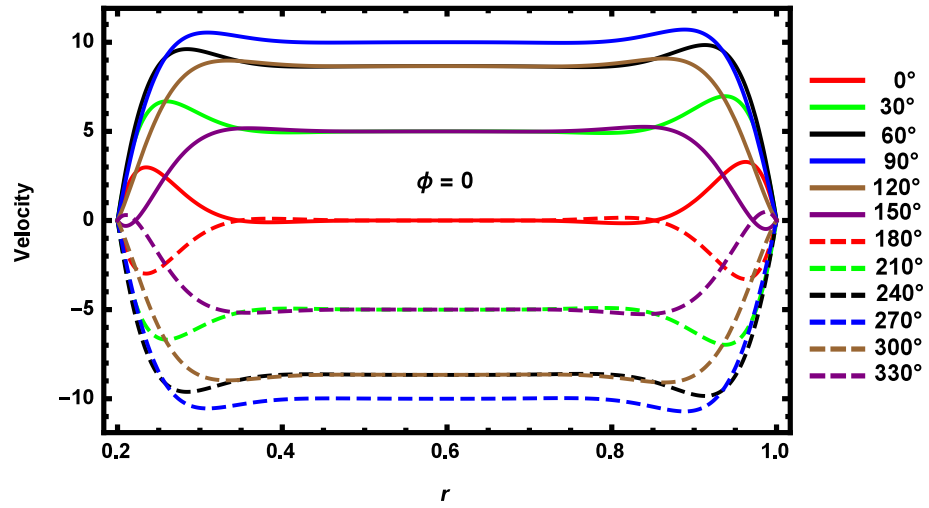
(a)



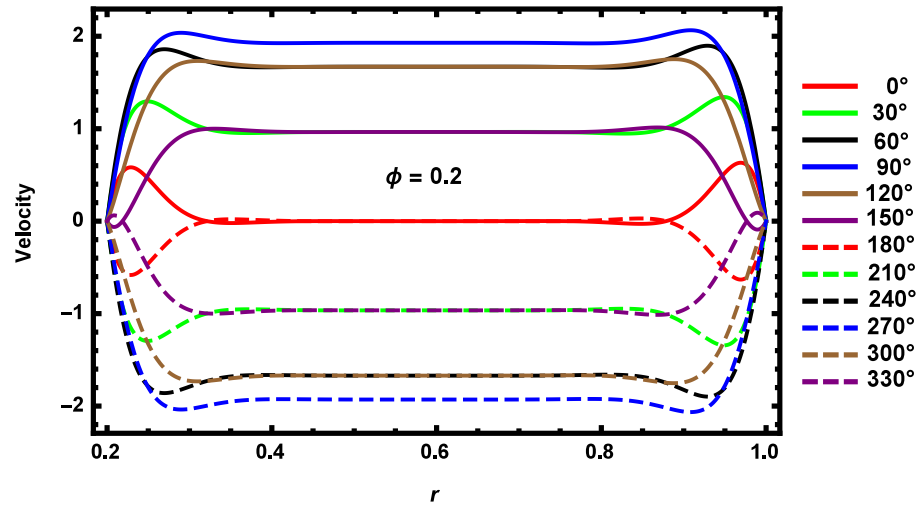
(b)

Figure 3.3: Velocity profile variance for $0^\circ \leq t \leq 360^\circ$ when $Re = 100$ and $M = 0$

Moreover, the velocity profile shows increasing behavior when Reynolds number escalate. When Reynolds number increases, viscous forces tends to decrease then as a result fluid particle movement becomes faster that causes steady increase in velocity profile as illustrated in Figs. 3.4(a)-(b).



(a)

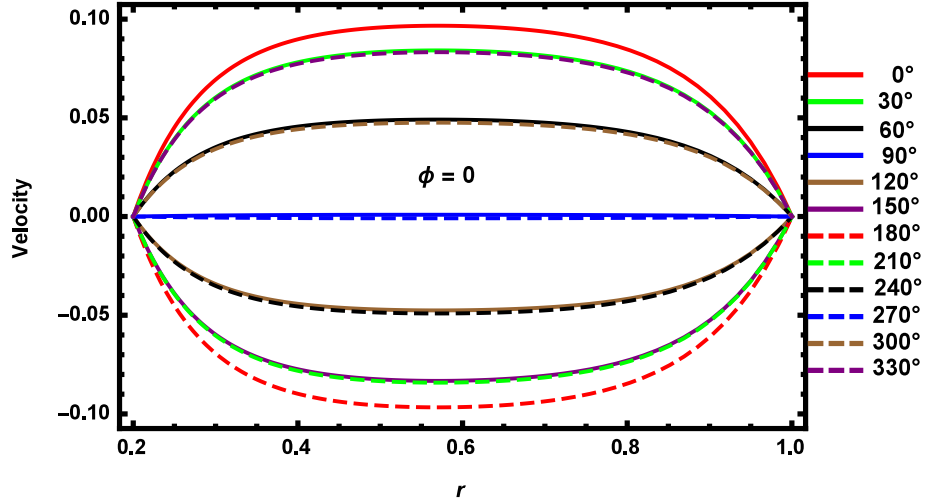


(b)

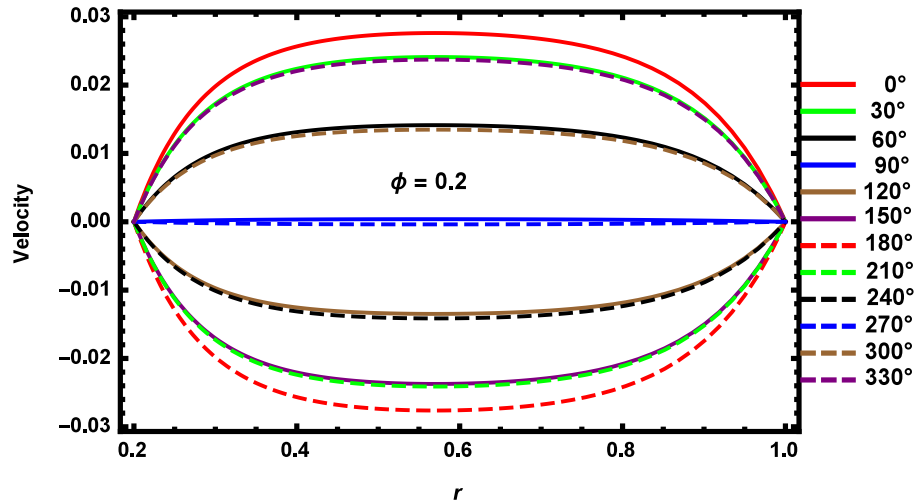
Figure 3.4: Velocity profile variance for $0^\circ \leq t \leq 360^\circ$ when $Re = 900$ and $M = 0$.

In Figures 3.5(a)-(b) Hartmann number (M) impact on velocity profile for both base fluid and nanofluid can be observed in comparison of Figs 3.4(a)-(b). For $M = 0$, Figs 3.4(a)-(b) shows the velocity distribution is adjacent along the duct walls. Figures 3.5(a)-(b) claimed that for $M = 10$, velocity profile follows a parabolic path and

highest amplitude is observed at mean position. The amplitude of the velocity profile compressed when Hartmann number increases, also the inclusion of nanoparticles reduce maximum velocity for base fluid as observed in Fig 3.5(b). The flow rate decreases due to retardant behavior of magnetic field.



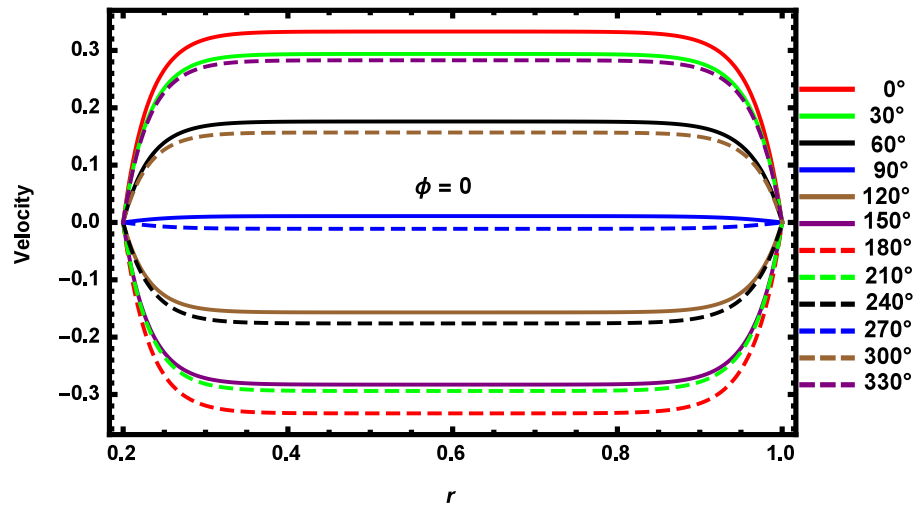
(a)



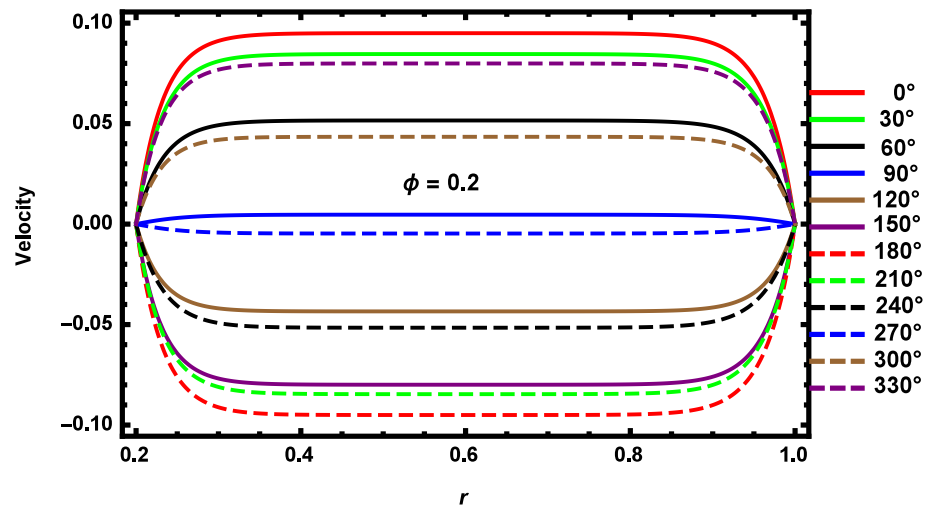
(b)

Figure 3.5: Velocity profile variance for $0^\circ \leq t \leq 360^\circ$ when $Re = 1$ and $M = 10$.

The variation in velocity profile for both base fluid and nanofluid for large values of Reynolds number and Hartmann number is depicted in Figs 3.6(a)-(b). It is observed that magnetic field serves as a resistant force for a fluid flow which results in a reduction of flow rate. Moreover, the annular effect which is a trait of pulsatile flow, is suppressed by the magnetic field.



(a)



(b)

Figure 3.6: Velocity profile variance for $0^\circ \leq t \leq 360^\circ$ when $Re = 30$ and $M = 30$.

The velocity increases as the flow area decreases, as observed in Figs 3.7 and 3.8 (a)-(c), increment in nanoparticles volume fraction (ϕ) turns to reduce velocity. For different values of radius, the flow region formed a series of envelopes, and the velocity field acquired its highest place as radius increases. Inner cylinder radius is less than or equal to the outer cylinder radius, thus the velocity profile domain is restricted between $0 \leq r \leq 1$. As a result, the maximum velocity appears in the vicinity of ducts for flow areas ranging from 0.7 to 1, and the annular effect decreases as the flow area decreases. Figures 3.8 (a)-(c) revealed that velocity profile gradually decreases as the nanoparticle volume fraction increases. For base fluid ($\phi = 0$) maximum velocity distribution is observed in Fig 3.7.

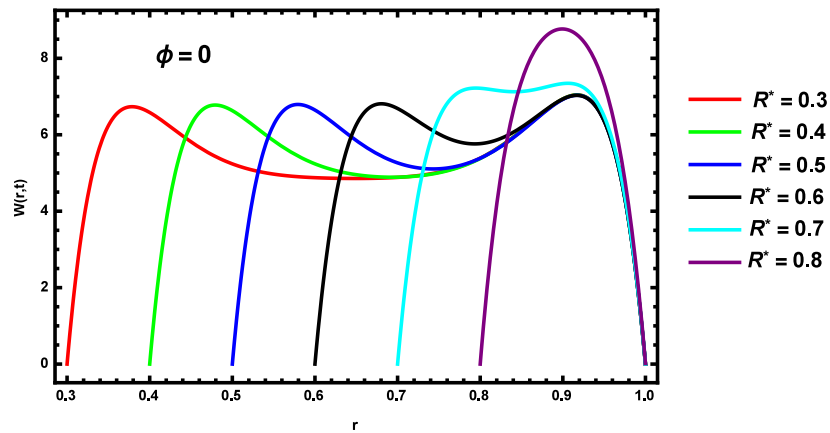


Figure 3.7: For base fluid, R^* influence on velocity profile when $Re = 400$ and $t = 30$.

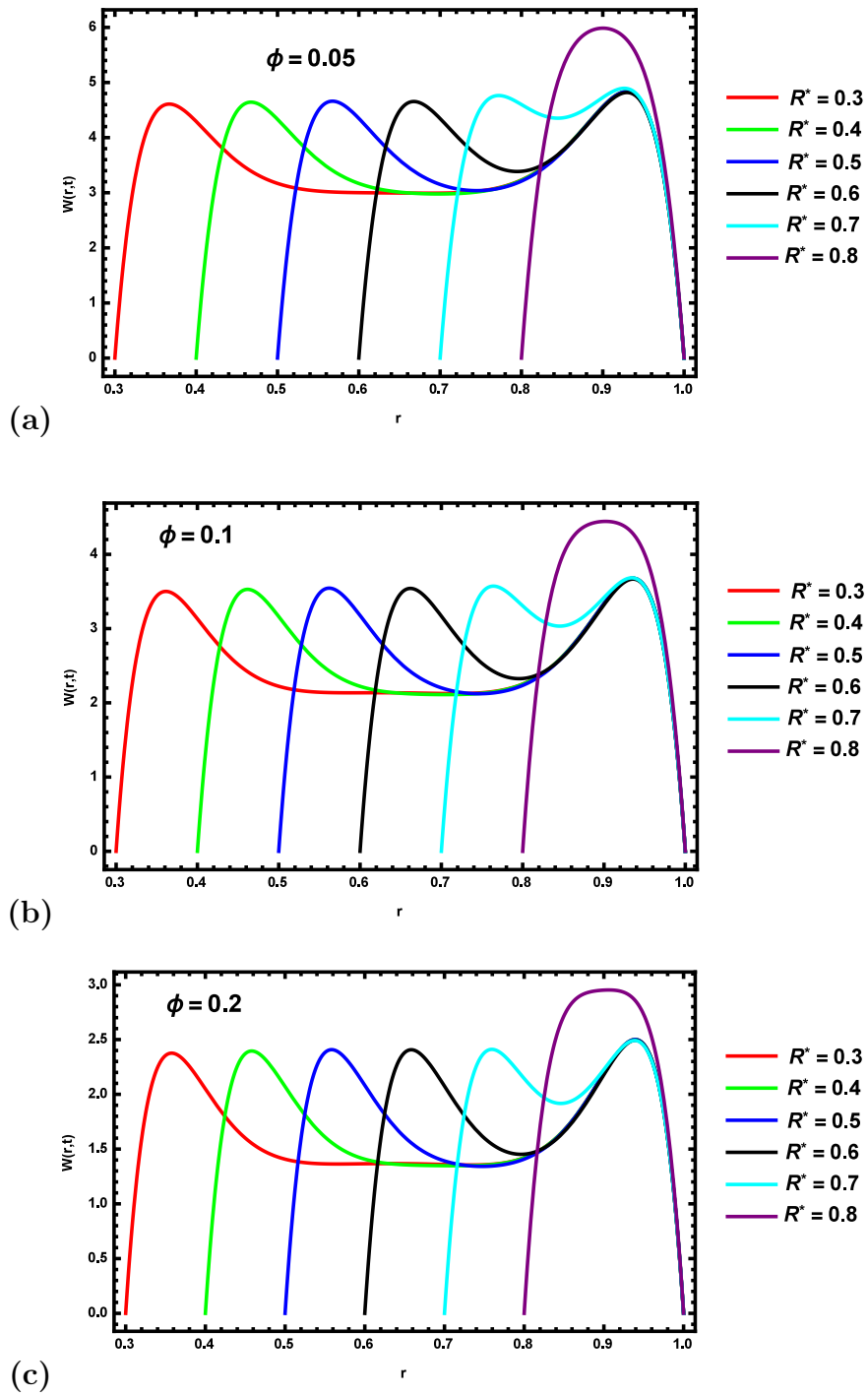


Figure 3.8: R^* influence on velocity profile for different ϕ when $Re = 400$ and $t = 30$.

3.3.2 Vortex

The outcomes of vortex profile obtained in current analysis are close to those presented by Majdalani [16]. Variations in vorticity radial profile, for varying choice of ϕ (nanoparticle volume fraction) is observed in Figs. 3.9 and 3.10(a)-(c). A vortex is an area in a fluid where the flow is spinning, straight or bended way around a pivot line. According to the vortex concept, the comparison shown in Figs 3.9 and 3.10 demonstrates that vortices magnitude is significantly stronger at the domain's extreme level. The vortex distribution becomes more compressed for increasing ϕ , as observed in Figs. 3.10(a)-(c). Further observations claimed that for varying choice of nanoparticle volume fraction, vortex of certain phases is set to be negative, which indicates the existence of backflow. Figure 3.9 illustrates that variations observed in vortex profile are higher for the base fluid ($\phi = 0$), rather than variations noticed for increasing values of ϕ in Figs 3.10(a)-(c).

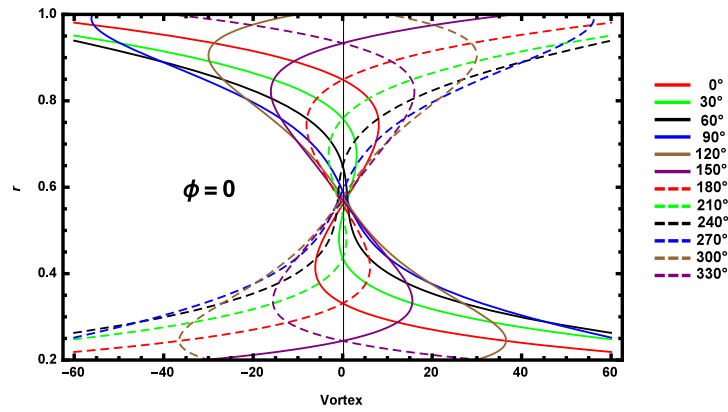


Figure 3.9: For base fluid, variance in vortex profile for $0^\circ \leq t \leq 360^\circ$ when $M = 5$ and $Re = 100$.

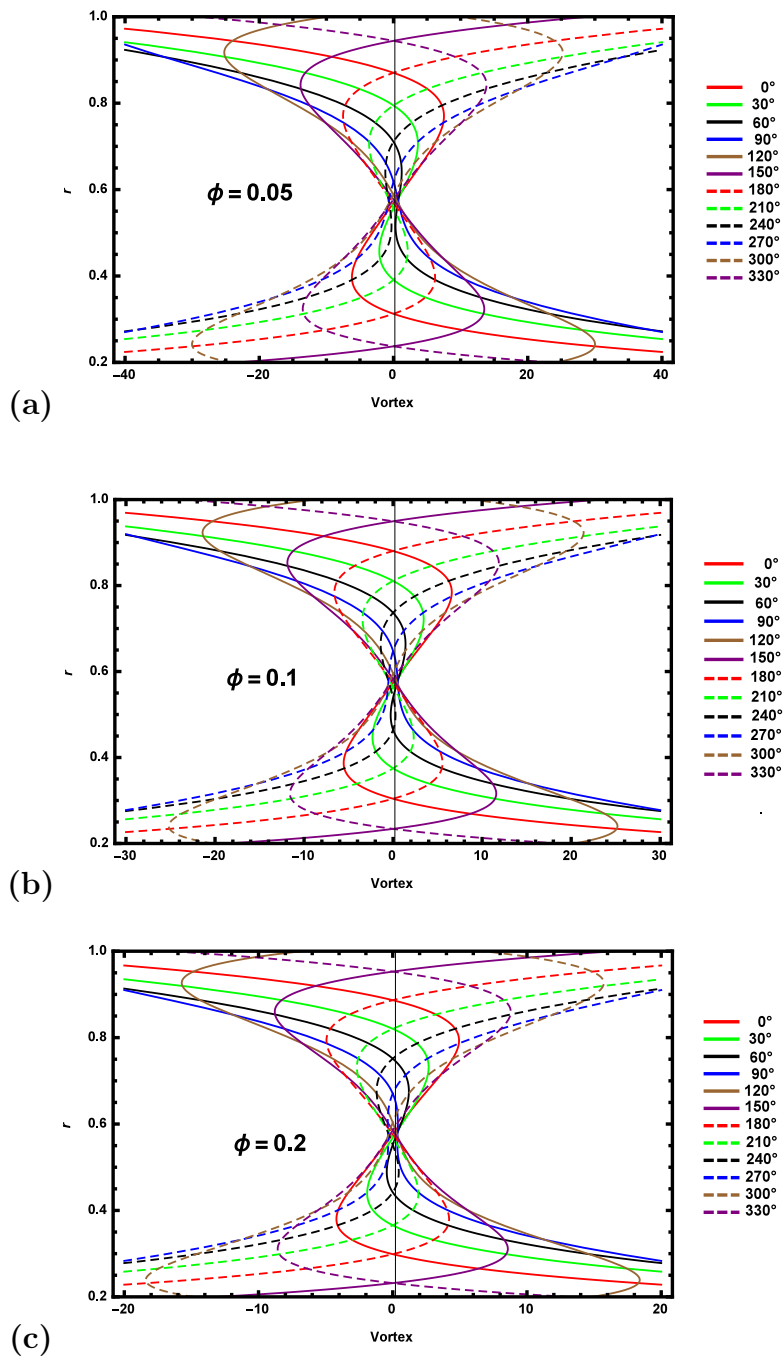


Figure 3.10: For different ϕ variance in vortex profile for $0^\circ \leq t \leq 360^\circ$ when $M = 5$ and $Re = 100$.

3.3.3 Pressure

Figure 3.11-3.12 depicts that for large values of ϕ , pressure gradient varies. Maximum pressure gradient is observed at cylinder's mean position with $t = 180^\circ$, but with decreasing behavior. Moreover, it is noticed that the pressure gradient is minimum for $t = 0^\circ$ and $t = 360^\circ$, but it measures increasing behavior as nanoparticle volume fraction ϕ increases. Figure 3.11 represents maximum change in pressure gradient for $R^* = 0.2$, rather than for $R^* = 0.4$ as claimed in Fig 3.12.

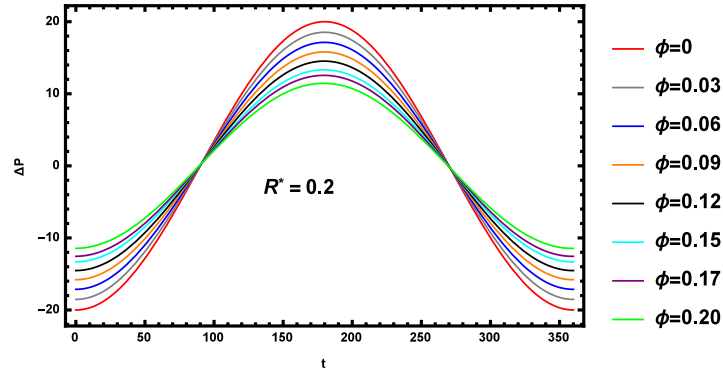


Figure 3.11: Pressure gradient at $R^* = 0.2$ when $Re = 100$ and $M = 30$.

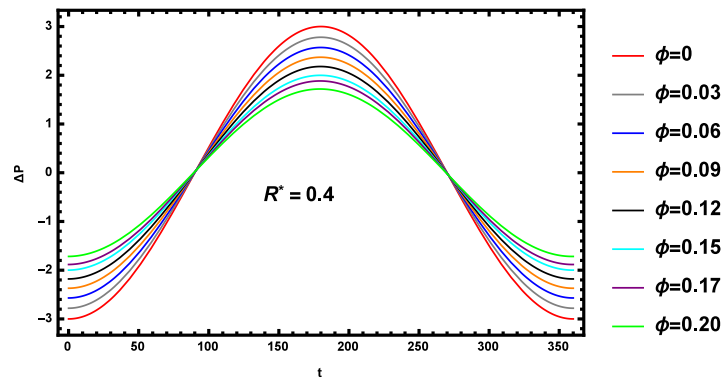


Figure 3.12: Pressure gradient at $R^* = 0.4$ when $Re = 100$ and $M = 30$.

3.3.4 Temperature

The analysis of heat transfer turns around the study of temperature profile located near cylinder's surface. Figures (3.13)-(3.16) portrays the variation in temperature profile against different parameters like Prandtl number (Pr), Hartmann number (M), Reynolds number (Re), pressure gradient amplitude (A), and nanoparticle volume fraction (ϕ). In Figs 3.13 and 3.14 variation in temperature profile for various choices of R^* , are plotted against pressure gradient amplitude. In Fig 3.13 it is observed that at $R^* = 0.1$ for large values of pressure gradient amplitude, temperature distribution of entire area of the two cylinders decreases. In Figs 3.14(a)-(b) for varying values of A , temperature profile at $R^* = 0.3$ and at $R^* = 0.5$ changes its behavior in decreasing manner. At $R^* = 0.7$, temperature profile turns its behavior twice as shown in Fig 3.14(c).

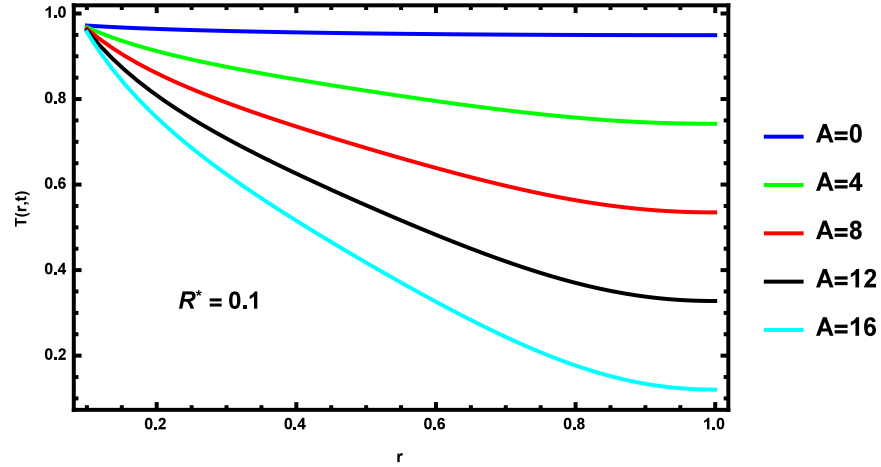


Figure 3.13: Pressure gradient (A) influence on temperature profile.

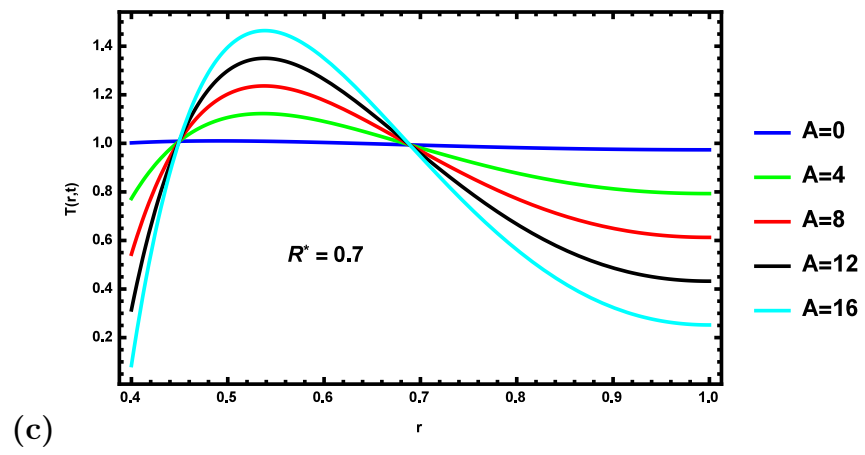
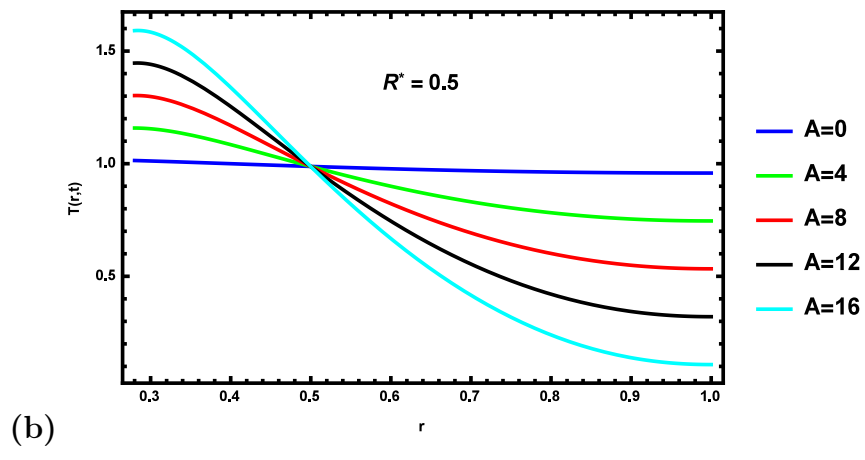
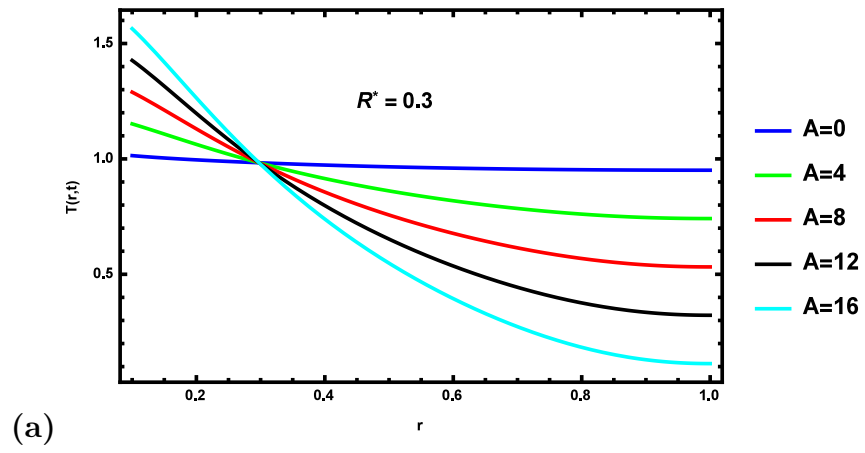


Figure 3.14: Pressure gradient (A) influence on temperature profile.

The temperature distribution of water-based copper nanoparticles changes with nanoparticle volume fraction (ϕ) as observed in Fig. 3.15. It is found that rate of heat transfer escalates with nanoparticle inclusion. Moreover, observations claimed that due to effective thermal conductivity, heat transfer rate of water-based copper nanoparticles is higher than the base fluid. Figure 3.16(a) represents Hartmann number (M) influence on temperature profile. The implementation of transverse magnetic field tends to rise fluid temperature. Magnetic field induces an electric current in a fluid that causes to generate heat in a fluid. As a result magnetic field radiation helps to improve enhancement process. The time influence on temperature profile is depicted in Figs 3.16(b)-(c), it is observed that temperature profile has increasing behavior for large values of time (t).

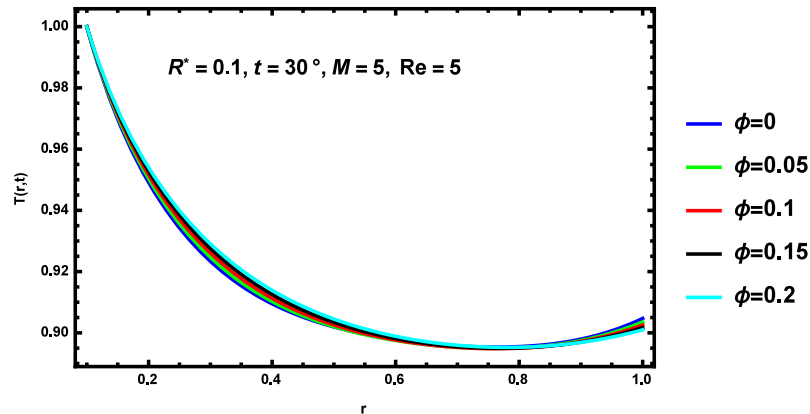


Figure 3.15: Nanoparticle volume fraction (ϕ) influence on temperature profile.

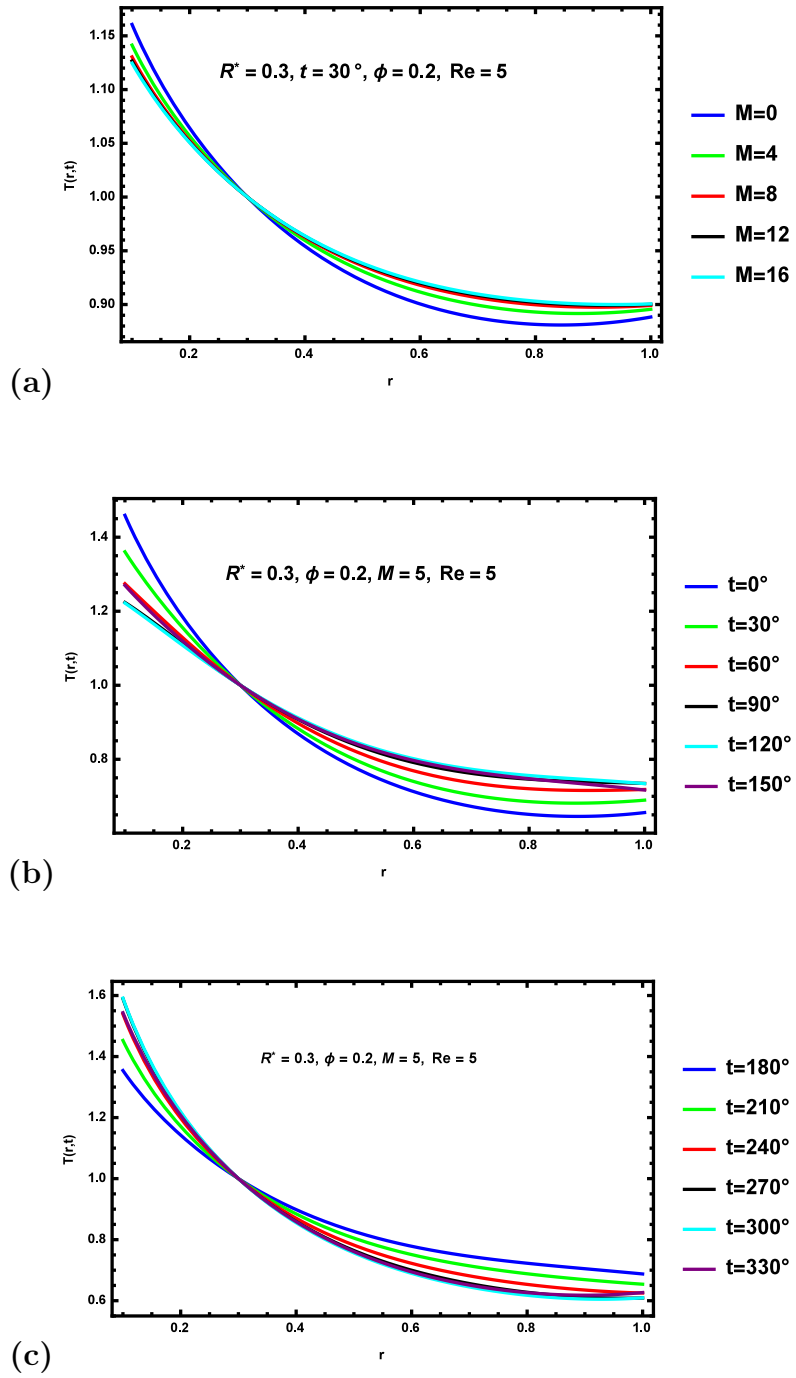


Figure 3.16: (a) Hartmann number and (b-c) time influence on temperature profile.

Chapter 4

Heat transfer and nanofluids MHD flow across stretching cylinder

This chapter covers the review of [35]. It describes MHD flow of nanofluids and heat transfer through a stretching cylinder. Copper, titanium oxide, silver, and alumina nanoparticles are considered alongwith water as base fluid. Tiwari and Das [41] nanofluid model is adopted. MATLAB package *bvp4c* is implemented to obtain numerical solution of flow governing equations. Furthermore, outcomes of the parameters governing the problem are analysed.

4.1 *bvp4c*

Flows occuring in physical world are governed by complex non linear PDEs. In order to get a solution MATLAB programs require the user to provide with the initial guesses for the solution required and also for parameters involved in the governing equations. The choice of initial guess vector plays an important role to find aproximate solution

of interest. MATLAB built in package *bvp4c*, which implements collocation method, is capable of solving non-linear problems. A boundary value problem can have several solutions therefore, it is required to provide initial guess. Selecting a suitable guess for a specific interval of interest is challenging, the problem is initially solved on a smaller interval. Later on, problem is then extended to particular interval of interest after an appropriate initial guess has been obtained. The computations needed to obtain a numerical solution are extensively influenced by the initial guess. For detailed discription of this frame work, references [43]-[44] can be consulted.

4.2 Mathematical formulation

The problem under consideration surrounds an incompressible, laminar, steady flow of an electrically conducting fluid. Flow occurs due to stretched cylinder with radius a^* . Fluid has no movement in axial direction, r -axis measures the radial direction and z -axis measures along cylinder axis, as shown in Fig. 4.1. [35]. In radial direction uniform magnetic field is applied that has no influence on induced magnetic field. $T_w > T_\infty$, where T_∞ is ambient fluid temperature and surface temperature T_w is constant. Ohmic heating, viscous dissipation, magnetic Reynolds number are omitted as they are presumed to be small. Nanoparticles (Cu, TiO_2, Ag, Al_2O_3) and basefluid (water) with no slip condition is assumed to be in thermal equilibrium. Table 4.1 lists the thermophysical characteristics of nanofluids.

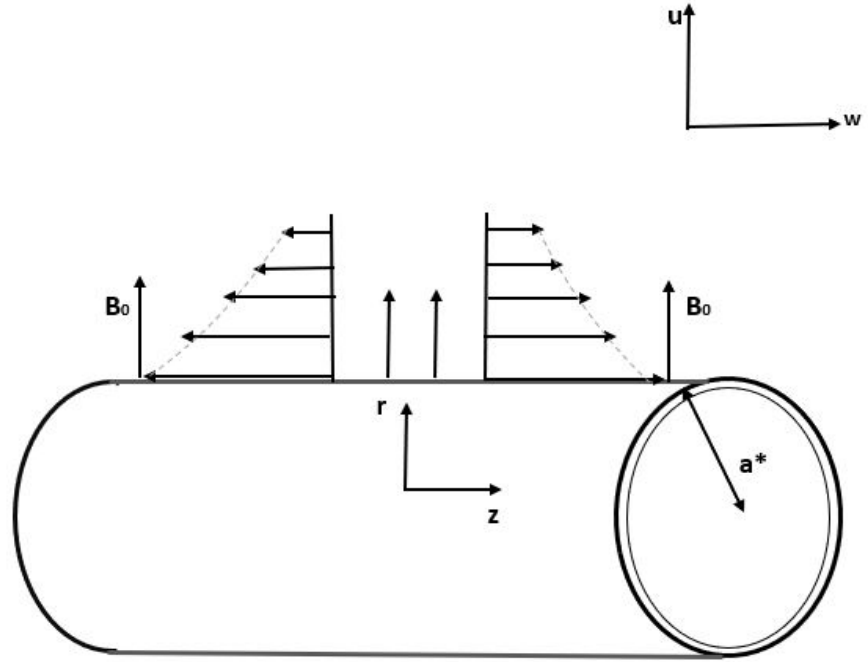


Figure 4.1: Physical configuration and coordinate system.

Table 4.1: Thermophysical characteristics of various nanoparticles and basefluid (water). [45].

Phase	$\rho(Kg/m^3)$	$k(W/mK)$	$C_p(J/kgK)$	$\beta \times 10^5(K^{-1})$
H_2O	997.1	0.613	4,179	21
Ag	10,500	429	235	1.89
Cu	8,933	401	385	1.67
TiO_2	4,250	8.9538	686.2	0.9
Al_2O_3	3,970	40	765	0.85

Accounting these assumptions and following Tiwari and Das model [41], fluid flow

governing equations over a stretching cylinder are:

$$\frac{\partial(ru)}{\partial r} + \frac{\partial(rw)}{\partial z} = 0, \quad (4.1)$$

$$\rho_{nf} \left(u \frac{\partial u}{\partial r} + w \frac{\partial u}{\partial z} \right) = -\frac{\partial p}{\partial r} + \mu_{nf} \left[\frac{\partial^2 u}{\partial r^2} + \frac{1}{r} \frac{\partial u}{\partial r} - \frac{u}{r^2} \right], \quad (4.2)$$

$$\rho_{nf} \left(u \frac{\partial w}{\partial r} + w \frac{\partial w}{\partial z} \right) = \mu_{nf} \left[\frac{\partial^2 w}{\partial r^2} + \frac{1}{r} \frac{\partial w}{\partial r} \right] - \sigma_{nf} B_o^2 w, \quad (4.3)$$

$$\left(u \frac{\partial T}{\partial r} + w \frac{\partial T}{\partial z} \right) = \frac{\kappa_{nf}}{(\rho c_p)_{nf}} \left[\frac{\partial^2 T}{\partial r^2} + \frac{1}{r} \frac{\partial T}{\partial r} \right], \quad (4.4)$$

where $(\rho c_p)_{nf}$, κ_{nf} , ρ_{nf} , σ_{nf} , and μ_{nf} are heat capacitance, thermal conductivity, effective density, electrical conductivity, and effective dynamic viscosity of nanofluid respectively.

$$\sigma_{nf} = (1 - \phi) \sigma_f + \phi \sigma_s \quad (4.5)$$

Mathematical expression of nanofluid properties can be seen in Eqs. (2.28)-(2.31) and Eq. (4.5). For this mathematical model boundary conditions assumed are given below:

$$\begin{aligned} u &= u_w, & w &= w_w, & T &= T_w, & \text{at} & \quad r = a^*. \\ w &\rightarrow 0, & T &\rightarrow T_\infty, & \text{as} & \quad r \rightarrow \infty, \end{aligned} \quad (4.6)$$

where, T is the fluid temperature, $u_w = 0$ and $w_w = 2bz$ for any positive integer b . u is velocity component in radial direction and w in axial direction.

Wang [42] showed that the governing Eqs. (4.3)-(4.4) are reduceable into ODEs by

following transformations:

$$\eta = \left(\frac{r}{a^*}\right)^2, \quad u = -ba^* \left(\frac{f(\eta)}{\sqrt{\eta}}\right), \quad w = 2bf'(\eta)z, \quad \theta(\eta) = \frac{T - T_\infty}{T_w - T_\infty}, \quad (4.7)$$

Eqs. (4.3)-(4.4) along with Eq. (4.6) will convert into following system via Eq. (4.7):

$$\text{Re.}(f'^2 - ff'').A_1.(1 - \phi)^{2.5} = \eta.f''' + f'' - f'.(1 - \phi)^{2.5}.M, \quad (4.8)$$

$$\left(1 + \frac{A_3}{A_4}.f.\text{Pr.Re}\right).\theta' + \eta.\theta'' = 0. \quad (4.9)$$

where prime indicates differentiation with respect to η . Transformed boundary conditions are:

$$\begin{aligned} f(1) &= 0, & f'(1) &= 1, & \theta(1) &= 1, \\ f'(\infty) &\rightarrow 0, & \theta(\infty) &\rightarrow 0. \end{aligned} \quad (4.10)$$

We have already discussed coefficients A_1 , A_3 and A_4 in Eq. (3.21) and Eq. (3.23)-(3.24). Prandtl number, magnetic parameter and Reynolds number are defined below:

$$Pr = \frac{\mu_f(\rho c_p)_f}{\kappa_f \rho_f}, \quad M = \frac{a^{*2}.\sigma_{nf}.B_o^2}{(4\mu_f)}, \quad Re = \frac{b.a^{*2}}{(2\nu_f)}. \quad (4.11)$$

Wall shear stress at the surface of cylinder are evaluated as follows:

$$\tau_w = \mu_{nf} \left(\frac{\partial w}{\partial r}\right)_{r=a^*} = \frac{\mu_f}{(1 - \phi)^{2.5}} \cdot \left[\frac{4bz.f''(1)}{a^*}\right]. \quad (4.12)$$

Eq. (4.12) can be used to evaluate skin friction C_f defined below:

$$C_f = \frac{\tau_w}{\rho_f w_w^2}. \quad (4.13)$$

Invoking transformation Eq. (4.7), Eq. (4.13) changes to the following form:

$$C_f \left(\frac{2z \cdot \text{Re}}{a^*} \right) = \frac{1}{(1 - \phi)^{2.5}} \cdot f''(1). \quad (4.14)$$

Cooling rate of surface can be determined by calculating Nusselt number defined below:

$$Nu = \frac{a^* q_w}{\kappa_f (T_w - T_\infty)}, \quad (4.15)$$

with wall heat flux as:

$$q_w = -\kappa_{nf} \left(\frac{\partial T}{\partial r} \right)_{r=a^*} = -\frac{2}{a^*} [\kappa_{nf} \cdot \theta'(1) \cdot (T_w - T_\infty)]. \quad (4.16)$$

Using Eq.(4.7) along with Eq. (4.16), Eq. (4.15) converts to the following fom:

$$Nu = -2 \cdot \frac{\kappa_{nf}}{\kappa_f} \cdot \theta'(1). \quad (4.17)$$

4.3 Numerical method

The boundary value problem given by Eqs. (4.8)-(4.9) along with boundary condition Eq. (4.10), is solved numerically by using MATLAB package *bvp4c*. Consider the

following substitution for obtaining the system of first order differential equations

$$\begin{aligned}
y_1 = f & \Rightarrow y'_1 = f' = y_2 \\
y_2 = f' & \Rightarrow y'_2 = f'' = y_3 \\
y_3 = f'' & \Rightarrow y'_3 = f''' = \frac{1}{\eta} \cdot [\text{Re} \cdot A_1 \cdot (1 - \phi)^{2.5} \cdot (y_2^2 - y_1 y_3) - y_3 \\
& \quad + M \cdot y_2 (1 - \phi)^{2.5}]. \tag{4.18}
\end{aligned}$$

$$\begin{aligned}
y_4 = \theta & \Rightarrow y'_4 = \theta' = y_5 \\
y_5 = \theta' & \Rightarrow y'_5 = \theta'' = -\frac{1}{\eta} \cdot (1 + \text{Re} \cdot \text{Pr} \cdot y_1 \cdot \frac{A_3}{A_4}) \cdot y_5 \tag{4.19}
\end{aligned}$$

Boundary conditions are:

$$\begin{aligned}
f(1) = 0 & \Rightarrow y_1(1) = 0 \\
f'(1) = 1 & \Rightarrow y_2(1) = 0 \\
f'(\infty) = 0 & \Rightarrow y_2(\infty) \rightarrow 0 \\
\theta(1) = 1 & \Rightarrow y_4(1) = 1 \\
\theta(\infty) \rightarrow 0 & \Rightarrow y_4(\infty) \rightarrow 0 \tag{4.20}
\end{aligned}$$

In order to solve Eqs. (4.18)-(4.19) with respective boundary conditions Eq. (4.20), we relied on the MATLAB built in function *bvp4c*. We initiate the computations by choosing small values. The computations are repeated several times until the initial slopes $f'''(1)$ and $\theta''(1)$ becomes consistent. The residuals in boundary condition for far from cylinder remains less than 10^{-6} . In Table 4.2 numerical evaluations are carried out to investigate grid independency for water based copper nanoparticles. For the current problem, 250 grid size is considered to have an independent solution. Table 4.3

demonstrates that obtained numerical results for $-\theta'(1)$ are in excellent match with those reported by Ishak [36] and Wang [42].

Table 4.2: Comparison of $-\theta'(1)$ for various mesh size when $M = 10$, $Pr = 6.2$, $\phi = 0.1$ and $Re = 7$.

Mesh size	50	100	150	200	250	300
$-\theta'(1)$	3.4868822	3.4868828	3.4868792	3.4868785	3.4868783	3.4868783

Table 4.3: Comparison with results of $-\theta'(1)$ obtained by Ishak [36] and Wang [42] when $Pr = 7$, $\phi = 0$ and $Re = 1$.

M	Present work	Ishak [36]	Wang [42]
0	2.05338	2.05338	2.05338
0.01	2.05213	2.05213	2.05338
0.05	2.04723	2.04723	2.05338
0.1	2.04121	2.04121	2.05338
0.5	1.99696	1.99696	2.05338

4.4 Results and discussion

In the presence of a magnetic field, fluid flow and heat transfer are analyzed numerically. An efficient computing platform *bvp4c* of MATLAB has been used to evaluate a representative problem given by Eqs. (4.8)-(4.9) with corresponding boundary conditions Eq. (4.10). To investigate flow behavior, effect of different non-dimensional parameters such as Reynolds number, nanoparticle volume fraction, and magnetic parameter for various nanofluids (Cu , Ag , TiO_2 and Al_2O_3) are displayed graphically in separate subsections. Re and ϕ influence on Nusselt number (Nu) and skin friction coefficient (C_f) is determined by Eq. (4.14) and Eq. (4.17).

4.4.1 Velocity

Velocity distribution against magnetic parameter and nanoparticle volume fraction are observed in Figs. (4.2)-(4.3). Figure 4.2 demonstrates that velocity profile tends to increase for increasing values of ϕ , due to increase in energy transmission. Magnetic parameter outcomes for velocity distribution is interpreted in Fig. 4.3. Velocity profile demonstrates that rate of transport decreases significantly when magnetic parameter increases, moreover study claimed that transport mechanism are opposed by transverse magnetic field. The Lorentz force induced by magnetic field tends to vary when magnetic parameter (M) changes due to magnetic field. As a result, Lorentz force causes transport phenomena to be more resistant. Higher magnetic parameter improved the resistance in flow region and thus velocity reduced, as presented in the Fig. 4.3.

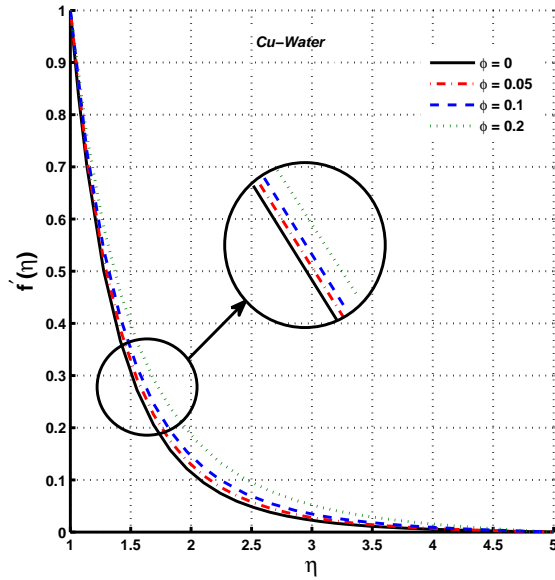


Figure 4.2: Variations in velocity distribution against ϕ .

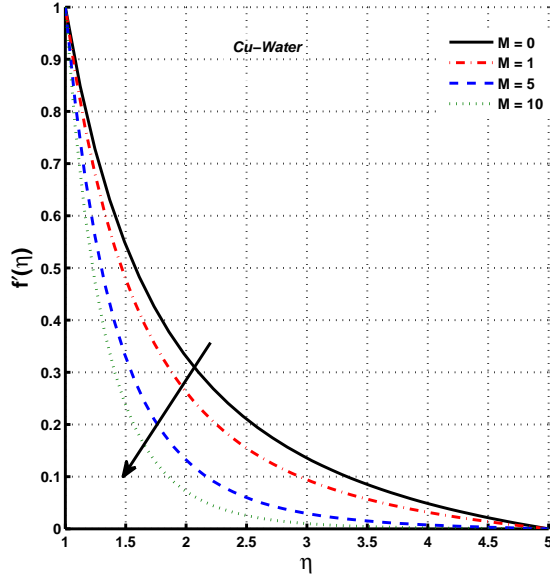


Figure 4.3: Variations in velocity distribution against M .

4.4.2 Temperature

Temperature distribution for magnetic parameter (M) and nanoparticle volume fraction (ϕ) is observed in Figs. (4.4)-(4.5). Temperature behavior against ϕ is analyzed in Fig. 4.4. Temperature enhances for increasing size of ϕ . For large values of nanoparticle volume fraction, thermal boundary layer accelerates which is associated to nanofluid thermal conductivity. Due to increased thermal conductivity, temperature profile will increase, as observed in Fig. 4.4. Figure 4.5 depicts higher temperature distribution against magnetic parameter (M). Increase in magnetic parameter tends to increase Lorentz force among liquid particles and thus temperature boosted. Variations in temperature profile is observed in Fig. 4.6 for various kind of nanofluids, when $Re = 1$, $Pr = 6.2$, $M = 5$, and $\phi = 0.1$. Illustrations shows that inclusion of Ag nanoparticles provides highest temperature, whereas lowest temperature is obtained for TiO_2

nanoparticles.

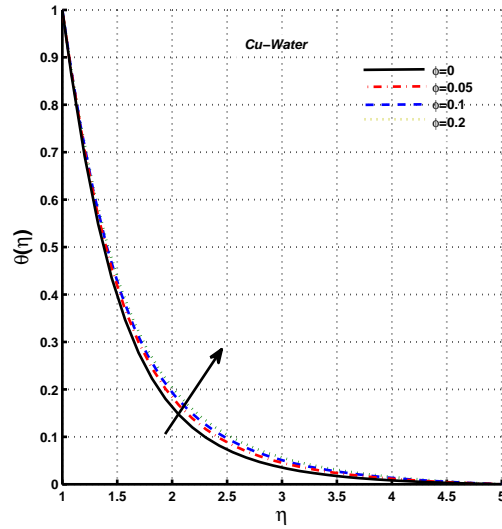


Figure 4.4: Temperature profile variance against ϕ .

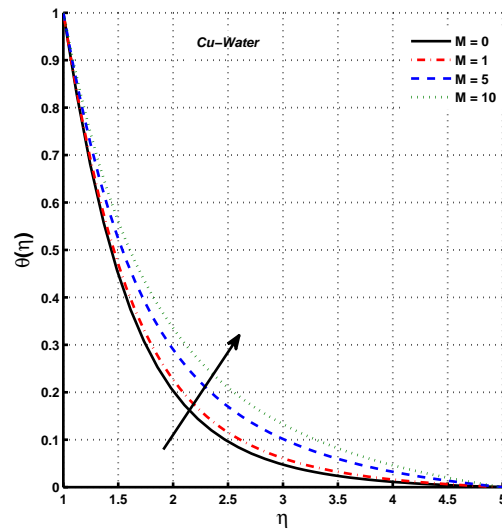


Figure 4.5: Temperature profile variance against M .

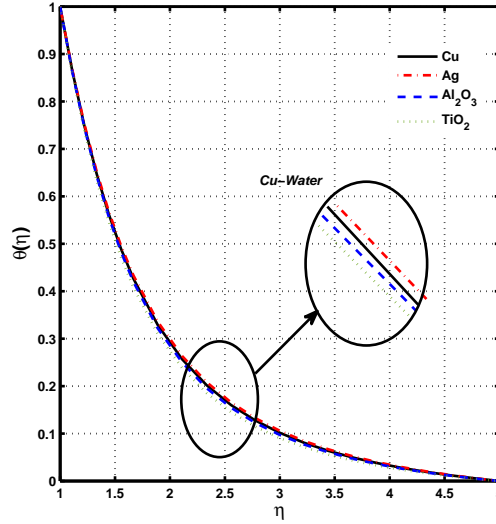


Figure 4.6: Temperature distribution for different nanofluids.

4.4.3 Skin friction coefficient and Nusselt number

Nusselt number (Nu) and skin friction coefficient (C_f) behavior for different parameters are observed in Figs. (4.7)-(4.10). It is noted that, C_f tends to increase for rising values of ϕ . Increasing values of magnetic parameter M will lead to increase absolute values of C_f , and this trend is prominent when values of ϕ is higher, as shown in Fig. 4.7. A stretching cylinder creates dragging force on the fluid. Due to this reason, skin friction coefficient (C_f) becomes negative. Skin friction coefficient for increasing values of Re and ϕ , changes its behavior from increasing to decreasing, as observed in Fig. 4.8.

For varying values of Re , Nusselt number behavior against ϕ is observed in Fig. 4.9. The product of thermal conductivity ratio and temperature gradient is Nusselt number, as stated in Eq. (4.17).

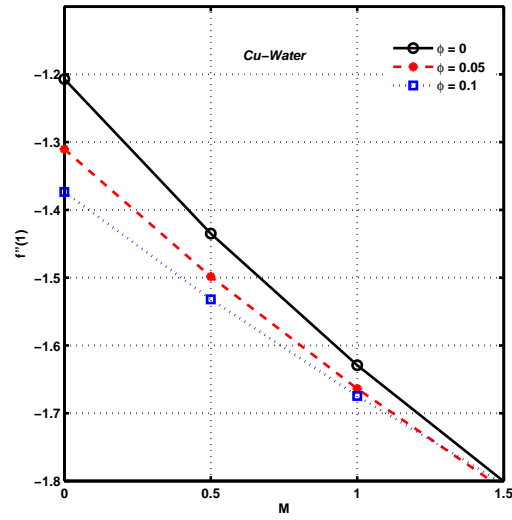


Figure 4.7: ϕ and M influence on skin friction coefficient.

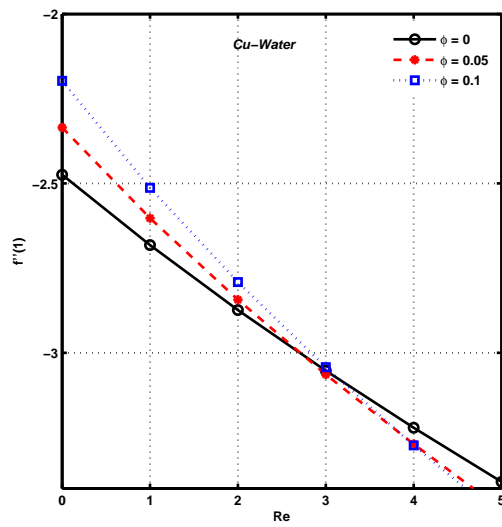


Figure 4.8: ϕ and Re influence on skin friction coefficient.

Observations revealed that Nu shows decreasing trend for large values of Reynolds

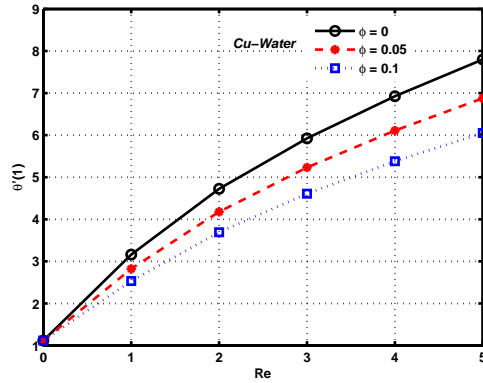


Figure 4.9: ϕ and Re Influence on Nusselt number.

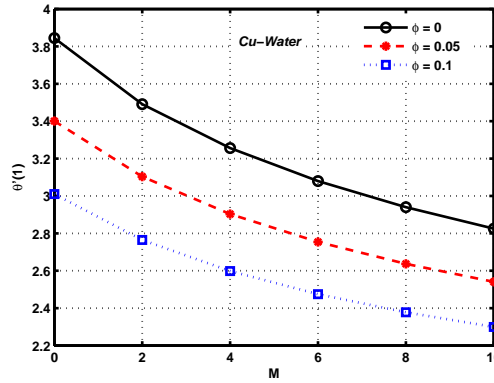


Figure 4.10: ϕ and M Influence on Nusselt number.

number and volume fraction, as depicted in Fig. 4.9. Reynolds number specifies the importance of inertia effect in comparison of viscous effect. For large magnetic parameter (M) and volume fraction (ϕ), Nusselt number shows decreasing behaviour as observed in Fig. 4.10.

For varying choice of nanofluids, the behavior of Nusselt number (Nu) and skin friction coefficient (C_f) are determined in Tables [4.4]-[4.7]. For different nanofluids, behavior of C_f and Nu varies accordingly. Also, for several kind of nanofluids heat transfer rate

acts differently. Observations claimed that TiO_2 nanoparticles have maximum Nu for different values of magnetic parameter M and nanoparticle volume fraction ϕ , whereas Ag nanoparticles yield lowest Nu . Furthermore, it is observed that, for all values of M , maximum amount of skin friction coefficient is obtained by Al_2O_3 nanoparticles. On contrary, Ag nanoparticles has less amount of it. Similar results are obtained in case of volume fraction.

Table 4.4: For various nanofluids, influence of Magnetic parameter on C_f , when $\phi = 0.1$, $Pr = 6.2$ and $Re = 1$.

M	Ag	Cu	TiO_2	Al_2O_3
0	-1.42198	-1.37341	-1.21583	-1.20571
1	-1.71397	-1.67442	-1.54958	-1.54176
5	-2.53869	-2.51306	-2.43474	-2.42997
10	-3.26517	-3.24561	-3.18638	-3.1828

Table 4.5: For various nanofluids, influence of M on Nu , when $Re = 1$, $Pr = 6.2$, and $\phi = 0.1$.

M	Ag	Cu	TiO_2	Al_2O_3
0	2.95132	3.01055	3.17749	3.09445
1	2.82047	2.87444	3.02409	2.94131
5	2.4903	2.53251	2.64709	2.57055
10	2.26468	2.2993	2.39238	2.32442

Table 4.6: For various nanofluids, influence of nanoparticle volume fraction on C_f , when $M = 5$, $Pr = 6.2$ and $Re = 1$.

ϕ	Ag	Cu	TiO_2	Al_2O_3
0.05	-2.61665	-2.60249	-2.55965	-2.55707
0.1	-2.53869	-2.51306	-2.43474	-2.42997
0.15	-2.44944	-2.41473	-2.30764	-2.30107
0.2	-2.34997	-2.3083	-2.17863	-2.17061

Table 4.7: For various nanofluids, influence of Nanoparticle volume fraction on Nu , when $Pr = 6.2$, $Re = 1$, and $M = 5$.

ϕ	Ag	Cu	TiO_2	Al_2O_3
0.05	2.79915	2.82399	2.88909	2.84628
0.1	2.4903	2.53251	2.64709	2.57055
0.15	2.22683	2.27964	2.43138	2.32801
0.2	2.00093	2.05838	2.23769	2.11282

Chapter 5

Darcy and radiation effect on heat transfer and MHD nanofluid flow across stretching cylinder

5.1 Introduction

Influence of heat transfer and radiation on nanofluid MHD flow with the effect of porous medium across a stretching cylinder is discussed in this chapter. Copper nanoparticles are considered alongwith water as a base fluid. Heat generation or absorption coefficient, Darcy parameter, and radiative heat flux are examined. Tiwari and Das [41] nanofluid model is adopted. A set of transformation is proposed, which transforms the governing problem into a coupled differential system, whose numerical solution is developed by MATLAB package *bvp4c*. For different parameters, variations in velocity and temperature distribution are analyzed graphically.

5.2 Mathematical formulation

The problem under consideration involves laminar, steady and an incompressible flow of nanofluid in a porous medium across stretching cylinder. Flow occurs due to stretching cylinder with radius a^* . There is no movement of fluid in axial direction. The r -axis measures radial direction and z -axis measures along tube axis as shown in Fig. 5.1.

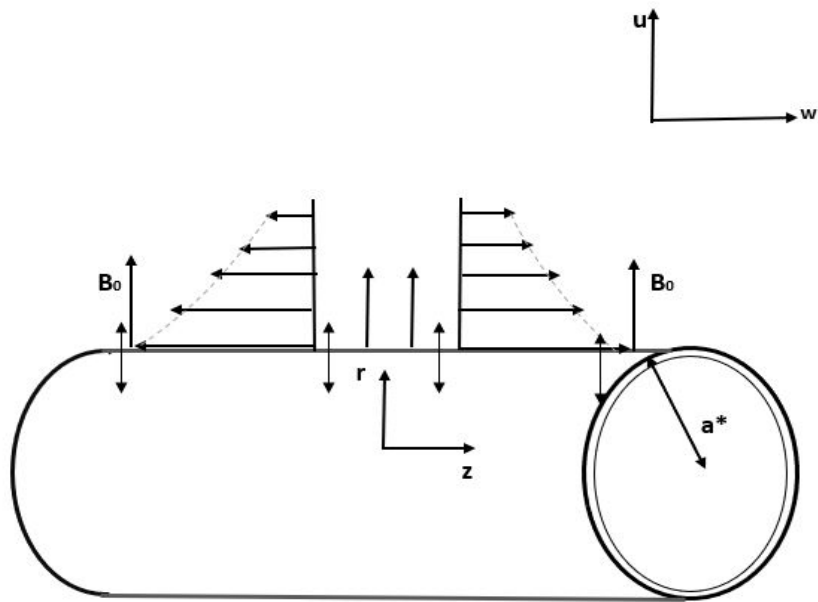


Figure 5.1: Physical model and coordinate system.

In radial direction uniform magnetic field is applied, and have no influence on induced magnetic field. $T_w > T_\infty$, where T_∞ is the temperature away from surface and surface temperature T_w is constant. Ohmic heating, viscous dissipation, magnetic Reynolds number are omitted as they are presumed to be small. Cu nanoparticles are considered

aling with water as a basefluid. Table 5.1 lists the thermophysical characteristics of nanofluids.

Table 5.1: Thermophysical characteristics of various nanoparticles and basefluid [45].

Phase	$\rho(Kg/m^3)$	$k(W/mK)$	$C_p(J/kgK)$	$\beta \times 10^5(K^{-1})$
H_2O	997.1	0.613	4,179	21
Ag	10,500	429	235	1.89
Cu	8,933	401	385	1.67
TiO_2	4,250	8.9538	686.2	0.9
Al_2O_3	3,970	40	765	0.85

Accounting these assumptions, fluid flow governing partial differential equations over a stretching cylinder are (see in Refs [46]- [47]):

$$\frac{\partial(ru)}{\partial r} + \frac{\partial(rw)}{\partial z} = 0, \quad (5.1)$$

$$\rho_{nf} \left(u \frac{\partial u}{\partial r} + w \frac{\partial u}{\partial z} \right) = -\frac{\partial p}{\partial r} + \mu_{nf} \left[\frac{\partial^2 u}{\partial r^2} + \frac{1}{r} \frac{\partial u}{\partial r} - \frac{u}{r^2} \right], \quad (5.2)$$

$$\rho_{nf} \left(u \frac{\partial w}{\partial r} + w \frac{\partial w}{\partial z} \right) = \mu_{nf} \left[\frac{\partial^2 w}{\partial r^2} + \frac{1}{r} \frac{\partial w}{\partial r} \right] - \sigma_{nf} B_o^2 w - \frac{\mu_{nf}}{K_o} w, \quad (5.3)$$

$$\left(u \frac{\partial T}{\partial r} + w \frac{\partial T}{\partial z} \right) = \frac{\kappa_{nf}}{(\rho c_p)_{nf}} \left[\frac{\partial^2 T}{\partial r^2} + \frac{1}{r} \frac{\partial T}{\partial r} \right] + \frac{Q_o(T - T_\infty)}{(\rho c_p)_{nf}} - \frac{1}{(\rho c_p)_{nf}} \frac{\partial q_r}{\partial r}, \quad (5.4)$$

where q_r is radiative heat flux. According to Rosseland approximation, q_r has the following expression:

$$q_r = -\frac{4}{3} \frac{\sigma^*}{k^*} \frac{\partial T^4}{\partial r} \quad (5.5)$$

In above equation k^* represents mean absorption coefficient and σ^* is Stefan-Boltzman constant. Assume that temperature variance within the flow is such that T^4 is expressed

in the form of Taylor series. Expand T^4 in Taylor series about T_∞ , ignore the higher order terms

$$T^4 \cong 4T_\infty^3 T - 3T_\infty^4. \quad (5.6)$$

For this model, boundary conditions are:

$$\begin{aligned} u = u_w, \quad w = w_w, \quad T = T_w, \quad \text{at} \quad r = a^*. \\ w \rightarrow 0, \quad T \rightarrow T_\infty, \quad \text{as} \quad r \rightarrow \infty. \end{aligned} \quad (5.7)$$

where $u_w = 0$ and $w_w = 2bz$ for any positive integer b . u is velocity component in radial direction and w in axial direction. T is nanofluid temperature, $(\rho c_p)_{nf}$, κ_{nf} , ρ_{nf} , σ_{nf} , and μ_{nf} are heat capacitance, thermal conductivity, effective density, electrical conductivity, and effective dynamic viscosity of nanofluid respectively.

Mathematical expression of above mentioned nanofluid properties can be seen in Eqs. (2.28)-(2.31) and Eq. (4.5). Similarity transformations given by Wang [42] are as follows:

$$\eta = \left(\frac{r}{a^*}\right)^2, \quad u = -ba^* \left(\frac{f(\eta)}{\sqrt{\eta}}\right), \quad w = 2bf'(\eta)z, \quad \theta(\eta) = \frac{T - T_\infty}{T_w - T_\infty}, \quad (5.8)$$

Invoking Eq. (5.8) into Eqs. (5.3)-(5.4) along with Eq. (5.7). Therefore, Eq. (5.3) becomes

$$\rho_f \cdot A_1 [4b^2 \cdot z (f'^2 - f \cdot f'')] = \frac{\mu_f}{(1 - \phi)^{2.5}} \left[\frac{4bz}{a^{*2}} (f''' + 2\eta \cdot f'''' + f''') \right] - \sigma_{nf} B_o^2 (2bf'(\eta)z)$$

or

$$\text{Re} \cdot (f'^2 - f f'') \cdot A_1 \cdot (1 - \phi)^{2.5} = \eta \cdot f'''' + f'' - f' \cdot (1 - \phi)^{2.5} \cdot M - K \cdot f'. \quad (5.9)$$

Proceeding Eq. (5.4):

$$\begin{aligned}
& 2bf'(\eta)z \cdot \frac{\partial(\theta(T_w - T_\infty) + T_\infty)}{\partial z} + \frac{-ba^* \cdot f(\eta)}{\sqrt{\eta}} \cdot \frac{\partial(\theta(T_w - T_\infty) + T_\infty)}{\partial r} \\
&= \frac{\kappa_{nf}}{(\rho c_p)_{nf}} \left[\frac{\partial^2(\theta(T_w - T_\infty) + T_\infty)}{\partial r^2} + \frac{1}{r} \cdot \frac{\partial(\theta(T_w - T_\infty) + T_\infty)}{\partial r} \right] + \frac{Q_o}{(\rho c_p)_{nf}} \cdot \theta(T_w - T_\infty) \\
&+ \frac{16}{3} \cdot \frac{\sigma^*}{k^*} \cdot \frac{T_\infty^3}{(\rho c_p)_{nf}} \cdot \left[\frac{\partial^2(\theta(T_w - T_\infty) + T_\infty)}{\partial r^2} \right], \\
&- \frac{ba^* \cdot f(\eta)}{\sqrt{\eta}} \cdot \theta'(T_w - T_\infty) \cdot \frac{2r}{a^{*2}} = \frac{A_4 \cdot \kappa_f}{A_3 \cdot (\rho c_p)_f} \cdot \left[\frac{2\theta'}{a^{*2}} (T_w - T_\infty) + \frac{1}{r} \cdot \frac{2r}{a^{*2}} \cdot \theta'(T_w - T_\infty) \right. \\
&+ \theta''(T_w - T_\infty) \cdot \frac{(2r)^2}{(a^{*2})^2} \left. \right] + \frac{Q_o}{A_3 \cdot (\rho c_p)_f} \cdot \theta(T_w - T_\infty) + \frac{16}{3} \cdot \frac{\sigma^*}{k^*} \cdot \frac{T_\infty^3}{A_3 \cdot (\rho c_p)_f} \cdot \left[\frac{2\theta'}{a^{*2}} \cdot (T_w - T_\infty) \right. \\
&+ \theta''(T_w - T_\infty) \cdot \frac{(2r)^2}{(a^{*2})^2} \left. \right], \\
&-2bf \cdot \theta' = \frac{A_4 \cdot \kappa_f}{A_3 \cdot (\rho c_p)_f} \cdot \left[\frac{4\theta'}{a^{*2}} + \frac{4\theta''}{a^{*2}} \cdot \eta \right] + \frac{Q_o \cdot \theta}{A_3 \cdot (\rho c_p)_f} + \frac{16}{3} \cdot \frac{\sigma^*}{k^*} \cdot \frac{T_\infty^3}{A_3 \cdot (\rho c_p)_f} \left[\frac{2\theta'}{a^{*2}} + \frac{4\theta''}{a^{*2}} \cdot \eta \right], \\
&- \frac{ba^{*2}}{2} \cdot \frac{A_3 \cdot (\rho c_p)_f}{A_4 \cdot \kappa_f} \cdot f \cdot \theta' = \theta' + \theta'' \cdot \eta + \frac{Q_o \cdot \theta \cdot a^{*2}}{4 \cdot A_4 \cdot \kappa_f} + \frac{16}{3} \cdot \frac{\sigma^*}{k^*} \cdot \frac{T_\infty^3}{A_4 \cdot \kappa_f} \cdot \left(\frac{\theta'}{2} + \theta'' \cdot \eta \right), \\
&-Re.Pr.f \cdot \theta' \cdot \frac{A_3}{A_4} = \theta' + \theta'' \cdot \eta + \frac{Q \cdot \theta}{A_4} + \frac{Nr}{A_4} \cdot \left(\frac{\theta'}{2} + \theta'' \cdot \eta \right), \\
&\theta'' \left(1 + \frac{Nr}{A_4} \right) \cdot \eta + \theta' \left(1 + \frac{Nr}{2A_4} + Re.Pr \cdot \frac{A_3}{A_4} \cdot f \right) + \frac{Q}{A_4} \cdot \theta = 0. \tag{5.10}
\end{aligned}$$

The coefficients A_1 , A_3 and A_4 are discussed in Eq. (3.21) and Eq. (3.23)-(3.24). The dimensionless parameters observed in Eq.(5.9) and Eq.(5.10) are as follows:

$$\begin{aligned}
Pr &= \frac{\mu_f(\rho c_p)_f}{\kappa_f \rho_f}, & M &= \frac{a^{*2} \cdot \sigma_{nf} \cdot B_o^2}{(4\mu_f)}, & Re &= \frac{b \cdot a^{*2}}{(2\nu_f)}, \\
K &= \frac{-a^{*2}}{4K_o}, & Nr &= \frac{16}{3} \cdot \frac{\sigma^*}{k^*} \cdot \frac{T_\infty^3}{\kappa_f}, & Q &= \frac{Q_o \cdot a^{*2}}{4 \cdot \kappa_f} \tag{5.11}
\end{aligned}$$

Now the boundary conditions (5.7) will transform to:

$$\begin{aligned} f(1) &= 0, & f'(1) &= 1, & \theta(1) &= 1, \\ f'(\infty) &\rightarrow 0, & \theta(\infty) &\rightarrow 0. \end{aligned} \quad (5.12)$$

Physical quantities of interest are C_f and Nu , given by Sheikholeslami [48]. At the cylinder's surface wall shear stress is evaluated as follows:

$$\tau_w = \mu_{nf} \left(\frac{\partial w}{\partial r} \right)_{r=a^*} = \frac{\mu_f}{(1-\phi)^{2.5}} \cdot \left[\frac{4bz \cdot f''(1)}{a^*} \right]. \quad (5.13)$$

Eq. (5.13) can be used to determine skin friction C_f defined below:

$$C_f = \frac{\tau_w}{\rho_f w_w^2}. \quad (5.14)$$

Using transformation Eq.(5.8), Eq. (5.14) changes to the following form:

$$C_f \left(\frac{2z \cdot Re}{a^*} \right) = \frac{1}{(1-\phi)^{2.5}} \cdot f''(1). \quad (5.15)$$

Cooling rate of surface can be determined by calculating Nusselt number defined below:

$$Nu = \frac{a^* q_w}{\kappa_f (T_w - T_\infty)}. \quad (5.16)$$

where q_w is wall heat flux and has following expression:

$$q_w = -\kappa_{nf} \left(\frac{\partial T}{\partial r} \right)_{r=a^*} = -\frac{2}{a^*} [\kappa_{nf} \cdot \theta'(1) \cdot (T_w - T_\infty)]. \quad (5.17)$$

Using Eq.(5.8) along with Eq. (5.17), Eq. (5.16) converts to the following fom:

$$Nu = -2 \cdot \frac{\kappa_{nf}}{\kappa_f} \cdot \theta'(1). \quad (5.18)$$

Table 5.2: Comparison of skin friction coefficient for various nanoparticles, when $\phi = 0.1$, $Pr = 6.2$, and $Re = 1$.

M	Ashorynejad [35]	Present work	Ashorynejad [35]	Present work
	Copper (<i>Cu</i>)		Silver (<i>Ag</i>)	
0	-1.37341	-1.37341	-1.42198	-1.42198
1	-1.67442	-1.67442	-1.71397	-1.71397
5	-2.51306	-2.51306	-2.53869	-2.53869
10	-3.24561	-3.24561	-3.26517	-3.26517
	Alumina (<i>Al₂O₃</i>)		Titanium oxide (<i>TiO₂</i>)	
0	-1.20571	-1.20571	-1.21583	-1.21583
1	-1.54176	-1.54176	-1.54958	-1.54958
5	-2.42997	-2.42997	-2.43474	-2.43474
10	-3.1828	-3.1828	-3.18638	-3.18638

Table 5.3: Comparison of Nusselt number for various nanoparticles, when $Re = 1$, $Pr = 6.2$, and $\phi = 0.1$.

M	Ashorynejad [35]	Present work	Ashorynejad [35]	Present work
	Copper (<i>Cu</i>)		Silver (<i>Ag</i>)	
0	3.01055	3.01055	2.95132	2.95132
1	2.87444	2.87444	2.82047	2.82047
5	2.53251	2.53251	2.4903	2.4903
10	2.2993	2.2993	2.26468	2.26468
	Alumina (<i>Al₂O₃</i>)		Titanium oxide (<i>TiO₂</i>)	
0	3.09445	3.09445	3.17749	3.17749
1	2.94131	2.94131	3.02409	3.02409
5	2.57055	2.57055	2.64709	2.64709
10	2.32442	2.32442	2.39238	2.39238

Table 5.2 and 5.3 demonstrates that obtained numerical results for skin friction coefficient and Nusselt number are in excellent match with those reported by [35].

5.3 Numerical method

The *bvp4c* method is used to perform numerical calculations for nonlinear ODEs. The system of first order for Eq. (5.9) and Eq. (5.10) along with boundary conditions Eq.(5.12) is given as:

$$\begin{aligned}
y_1 = f & \Rightarrow y'_1 = f' = y_2 \\
y_2 = f' & \Rightarrow y'_2 = f'' = y_3 \\
y_3 = f'' & \Rightarrow y'_3 = f''' = \frac{1}{\eta} \cdot [Re \cdot A_1 \cdot (1 - \phi)^{2.5} \cdot (y_2^2 - y_1 y_3) - y_3 \\
& \quad + M \cdot y_2 (1 - \phi)^{2.5} + K \cdot y_2]. \tag{5.19}
\end{aligned}$$

$$\begin{aligned}
y_4 = \theta & \Rightarrow y'_4 = \theta' = y_5 \\
y_5 = \theta' & \Rightarrow y'_5 = \theta'' = -\frac{1}{\eta(1 + \frac{Nr}{A_3})} \cdot [y_5(1 + \frac{Nr}{2 \cdot A_4} + Re \cdot Pr \cdot \frac{A_3}{A_4} \cdot y_1) \\
& \quad + \frac{Q}{A_4} \cdot y_4] \tag{5.20}
\end{aligned}$$

Boundary conditions will be:

$$\begin{aligned}
f(1) = 0 & \Rightarrow y_1(1) = 0 \\
f'(1) = 1 & \Rightarrow y_2(1) = 0 \\
f'(\infty) = 0 & \Rightarrow y_2(\infty) \rightarrow 0 \\
\theta(1) = 1 & \Rightarrow y_4(1) = 1 \\
\theta(\infty) \rightarrow 0 & \Rightarrow y_4(\infty) \rightarrow 0 \tag{5.21}
\end{aligned}$$

Eq. (5.19) and Eq. (5.20) gives system of first order along with boundary conditions Eq. (5.21).

5.4 Results and discussion

The behavior of associated flow variable for temperature and velocity distribution, rate of heat transfer and surface drag force with the effect of radiation parameter, porosity parameter, and heat generation or absorption parameter are analyzed in this section. Graphical and tabular results for Cu-water nanoparticles are observed for different physical parameters including porous medium parameter (K), nanoparticle volume fraction (ϕ), thermal radiation parameter (Nr), magnetic parameter (M), and heat generation or absorption parameter (Q).

5.4.1 Velocity

Porosity parameter influence on velocity distribution is observed in Fig. 5.1. For increasing values of porosity parameter, velocity profile decreases and as a result boundary layer thickness decelerate. Fig. 5.2 shows magnetic parameter influence on velocity profile. It is noted that with increasing values of M , velocity profile decreases and as a consequence boundary layer thickness deprecates. For large values of magnetic parameter, flow field resistance increases and as a result velocity decelerate. For greater values of ϕ , variance in velocity profile is observed in Fig. 5.3. Thickness of momentum boundary layer slightly escalates for large values of volume fraction.

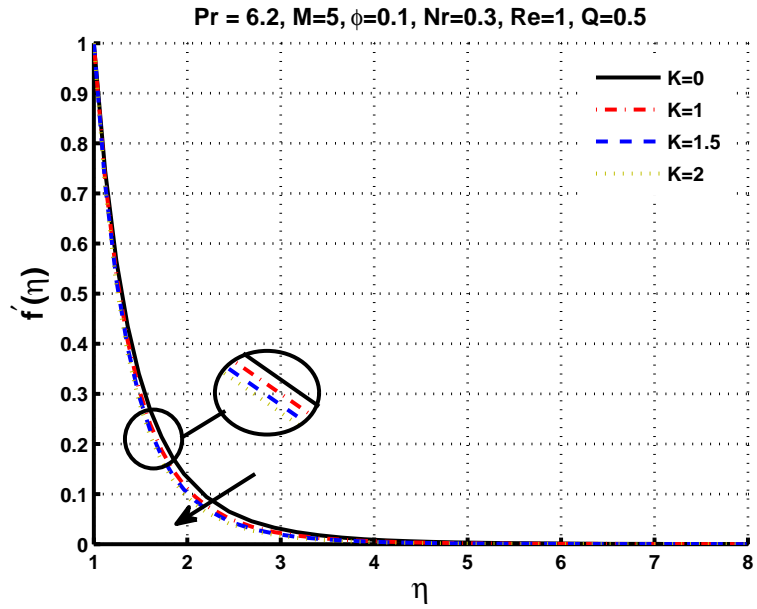


Figure 5.2: Velocity profile against porosity parameter.

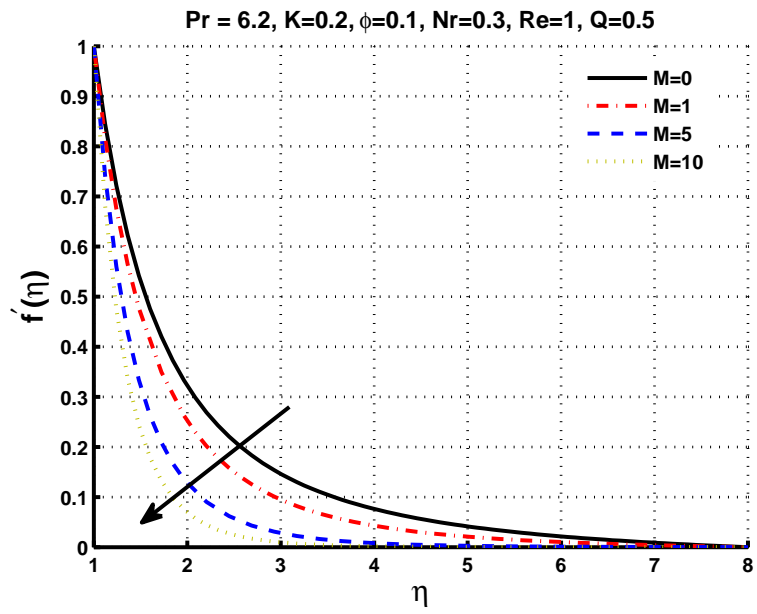


Figure 5.3: Velocity profile against M .

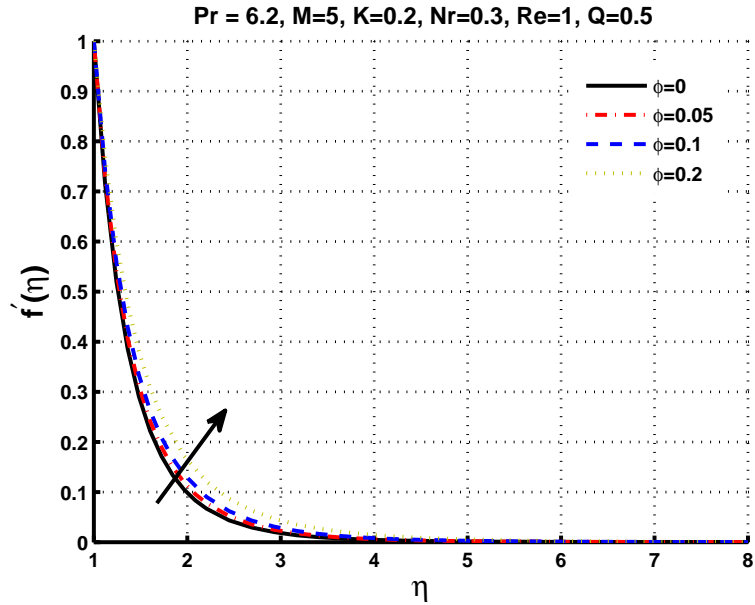


Figure 5.4: Velocity profile against varying choice of ϕ .

5.4.2 Temperature

For copper-water nanofluid, temperature profile for several controlling parameters are analyzed in Figs. (5.4)-(5.7). The variation in temperature profile against magnetic parameter is depicted in Fig. 5.4. Lorentz force tends to increase as the magnetic parameter grows and thus temperature boosted. In addition, thermal boundary layer thickness accelerates as values of M increases. Heat generation or absorption parameter influence on temperature distribution $\theta(\eta)$ is observed in Fig. 5.5. From observations one can say that, temperature increases for Q thus width of thermal boundary layer escalates. Figure 5.6 demonstrates radiation parameter effect on temperature profile. For greater values of Nr , thickness of thermal boundary layer accelerates and nanofluid temperature gradually increases. Figure 5.7 interprets impact of ϕ on temperature distribution. Thermal boundary layer thickness accelerates with increasing values of

ϕ , which is associated to nanofluids thermal conductivity. Therefore, due to increased thermal conductivity, temperature will increase as shown in Fig. 5.7.

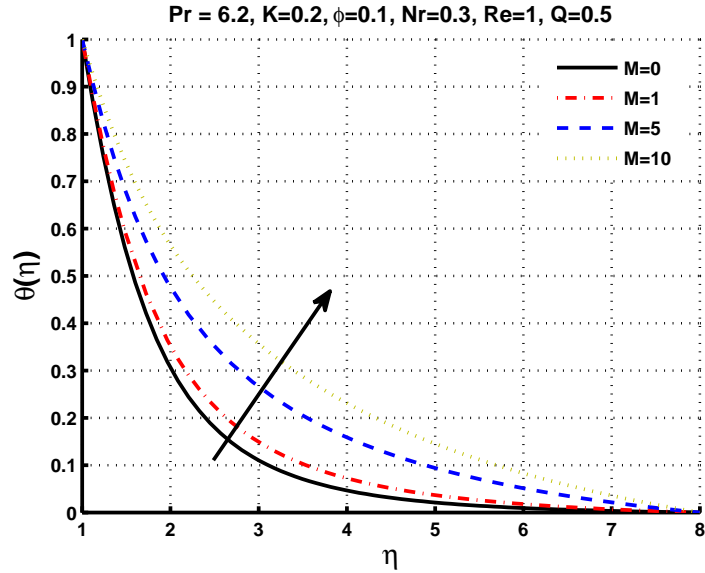


Figure 5.5: Temperature profile against M .

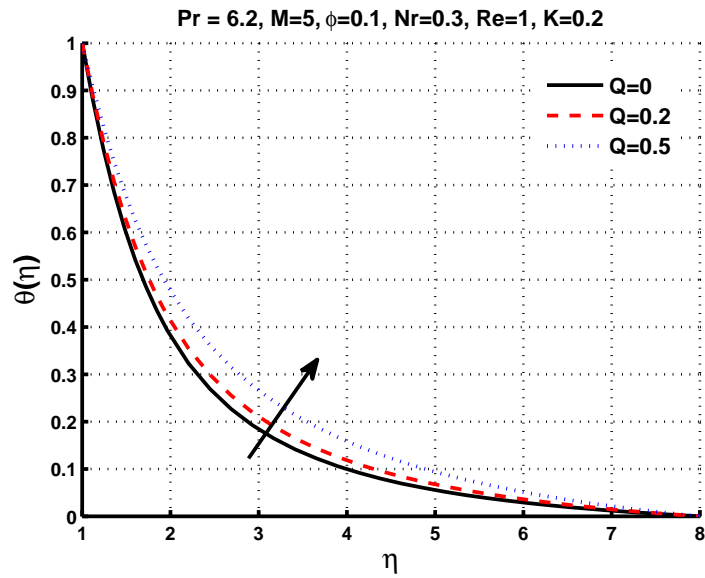


Figure 5.6: Temperature profile against Q .

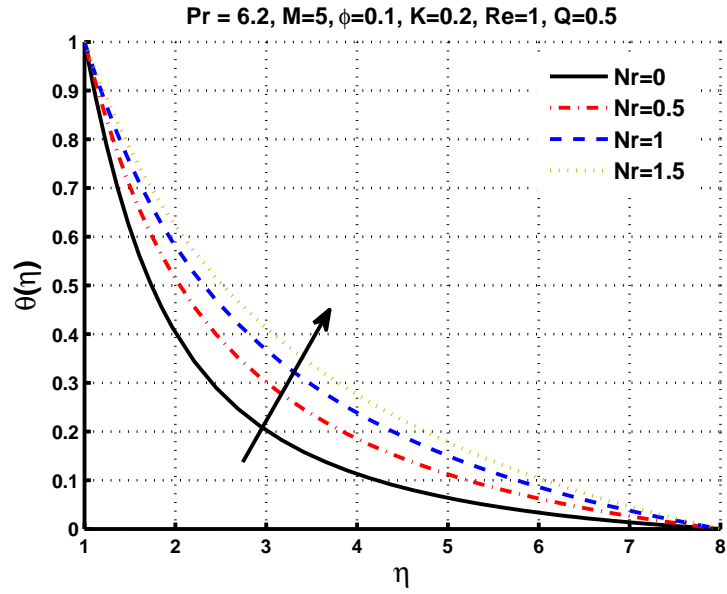


Figure 5.7: Temperature profile against Nr .

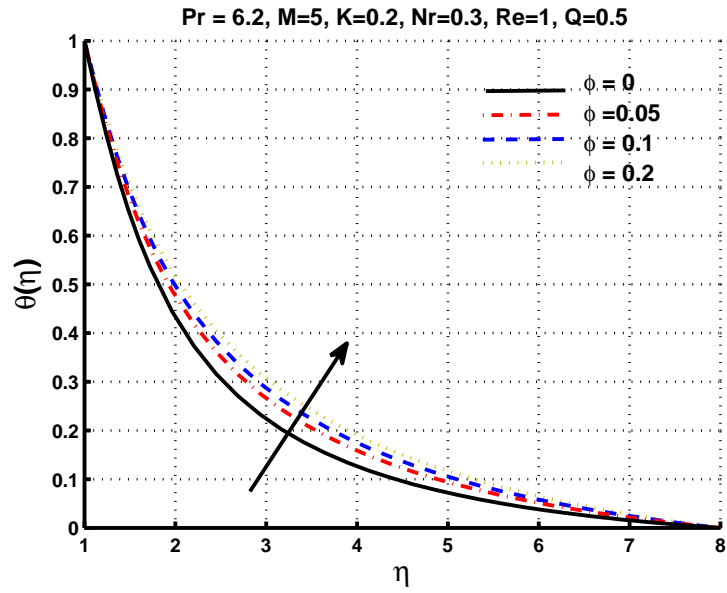


Figure 5.8: Temperature profile against ϕ .

5.4.3 Skin friction coefficient and Nusselt number

Outcomes of Nusselt number (Nu) and skin friction coefficient (C_f) for numerous governing parameters are observed in Figs. (5.8)-(5.12). For increasing values of K and ϕ , Nusselt number and skin friction coefficient possess opposite behavior. Nusselt number reduces and skin friction improves when size of nanoparticles increases as observed in Fig. 5.10 and Fig. 5.8. The influence of thermal radiation parameter along with nanoparticle volume fraction is observed in Fig. 5.11. Increment in volume fraction reduces the rate of heat transfer. Nu and C_f behavior for increasing values of heat source term and volume fraction is portrayed in Fig. 5.9 and Fig. 5.12. Increment in ϕ and Q tends to increase skin friction coefficient. Observations affirm that for greater values of Q and ϕ , Nusselt number (Nu) seems to have decreasing behavior.

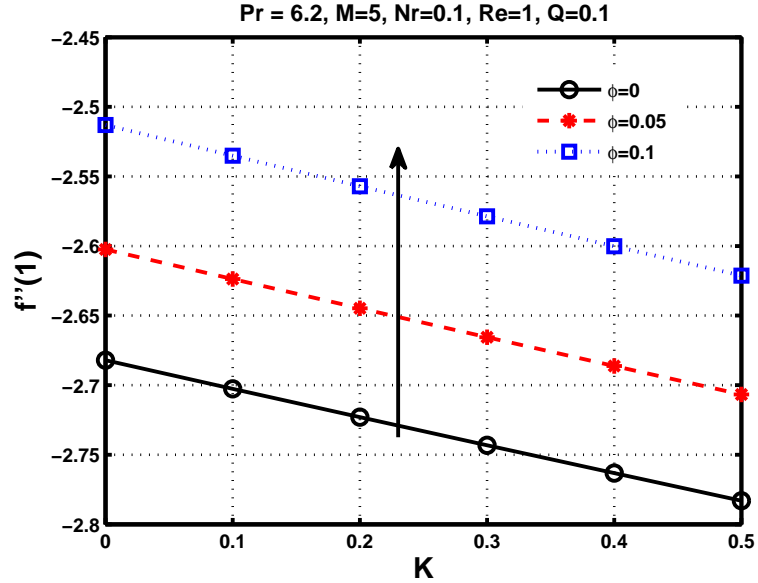


Figure 5.9: K and ϕ influence on skin friction coefficient.

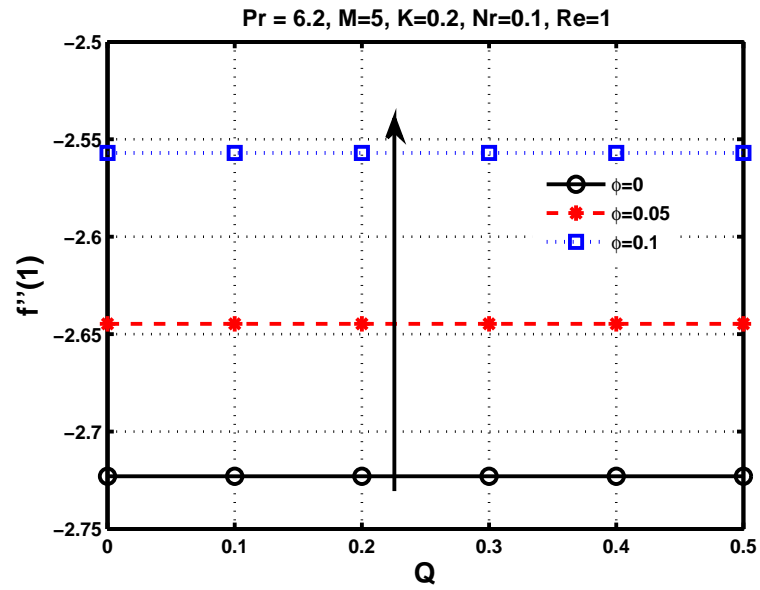


Figure 5.10: ϕ and Q influence on skin friction coefficient.

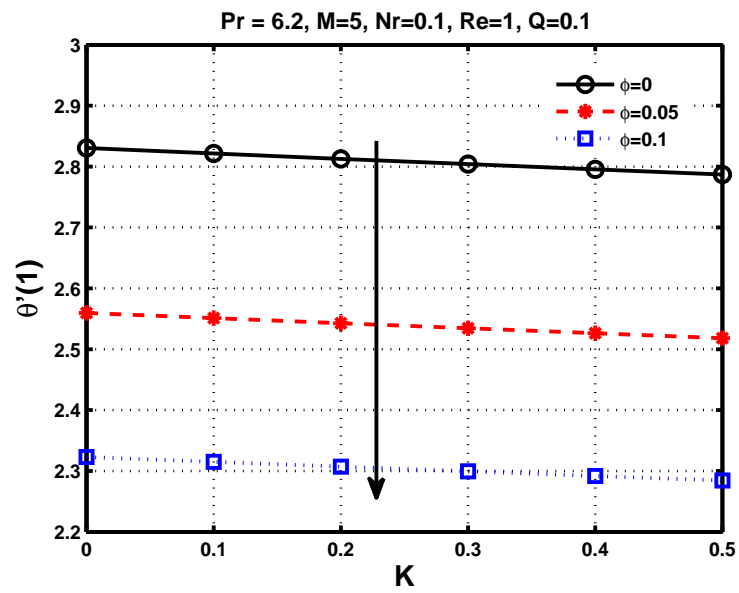


Figure 5.11: Nusselt number behavior for varying choices of ϕ and K .

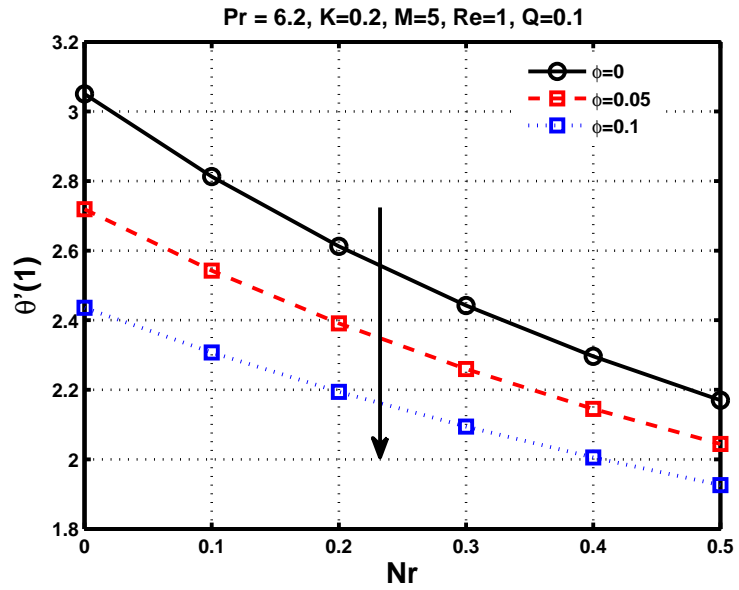


Figure 5.12: Nusselt number behavior for varying choices of ϕ and Nr .

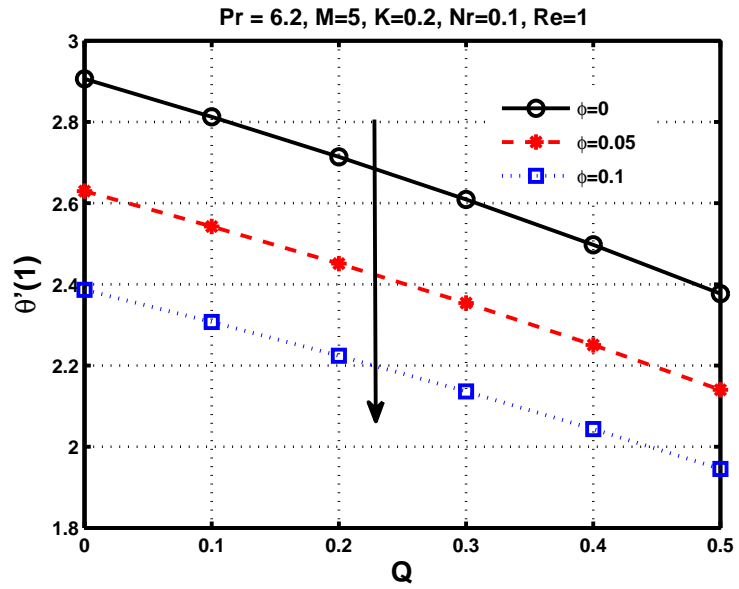


Figure 5.13: Nusselt number behavior for varying choices of Q and ϕ .

C_f and Nu behavior for different controlling parameters are tabulated in Table 5.2. Table 5.2 reveals that absolute values of C_f decreases as ϕ increases, whereas Nu exhibits opposite behavior. For magnetic parameter (M), absolute values of C_f elevates but Nu slows down gradually as M increases. Nusselt number decreases for large values of Nr and Q as observed in Table 5.2. Contrarily, Nr and Q has no influence on skin friction coefficient. With the effect of porosity parameter (K), Nu decelerates, whereas absolute values of C_f accelerates as K rises.

Table 5.4: Results of Nu and C_f for varying choices of ϕ, M, Nr, K and Q with $Re = 1$ and $Pr = 6.2$.

ϕ	M	Nr	K	Q	$f''(1)$	$-\theta'(1)$
0	5	0.1	0.2	0.1	-2.72298	2.81274
0.05					-2.64474	2.54267
0.1					-2.557	2.30715
0.2					-2.35659	1.91786
0.1	0	0.1	0.2	0.1	-1.45824	2.77267
	1				-1.7434	2.64062
	5				-2.557	2.30715
	10				-3.27886	2.07972
0.1	5	0.1	0.2	0.1	-2.557	2.30715
		0.2			-2.557	2.19408
		0.5			-2.557	1.92616
		1			-2.557	1.63261
0.1	5	0.1	0.1	0.1	-2.53514	2.31504
			0.2		-2.557	2.30715
			0.5		-2.62136	2.2843
			1		-2.72487	2.24864
0.1	5	0.1	0.2	0.1	-2.557	2.30715
				0.2	-2.557	2.22393
				0.5	-2.557	1.94514
				1	-2.557	1.32598

Chapter 6

Concluding Remarks

6.1 Water driven copper nanoparticles between two concentric cylinders with an oscillatory pressure gradient

Analysis of MHD flow of water based copper nanoparticles between two concentric cylinders is discussed in this thesis. For pulstaile flow exact solution of pressure, velocity and temperature distribution is obtained between concentric cylinders. For an extensive range of M , Re , and ϕ the solutions of temperature, pressure and velocity profiles are illustrated graphically. However, magnetic field impact on heat transfer investigated analytically. Most significant outcomes are listed below :

- Velocity amplitude possess decreasing trend for increasing values of nanoparticle volume fraction .
- Inclusion of copper nanoparticles tends to increase fluid temperature.

- Rate of heat transfer can be improved with the help of external magnetic field.

6.2 Heat transfer and nanofluids MHD flow across stretching cylinder

Mathematical model developed for steady two dimensional flow of an electrically conducting nanofluid across stretching cylinder has enabled us to determine volume fraction, Reynolds number, and magnetic parameter influence upon solution profiles. The important outcomes from the numerical analysis of the governing model are listed below:

- Increasing values of Reynolds number , nanoparticle volume fraction, and magnetic parameter results in the increment of absolute values of C_f .
- Nusselt number shows decreasing behavior for increasing values of nanoparticle volume fraction (ϕ) and magnetic parameter (M).
- Magnetic parameter (M) has opposite behavior for both velocity and temperature profiles. Velocity profile will decrease for increasing values of M , whereas temperature will increase.

6.3 Darcy and radiation effect on heat transfer and MHD nanofluid flow across stretching cylinder

Flow of an electrically conducting nanofluid in the presence of magnetic field across a stretching cylinder in a porous medium is numerically analyzed. The governing

PDEs are reduced to dimensionless ODEs using similarity transformations. Numerical solution of ODEs with appropriate boundary conditions has been acquired by using *bvp4c*. Influence of various controlling parameters such as heat generation or absorption coefficient (Q), nanoparticle volume fraction (ϕ), thermal radiation (Nr), magnetic parameter (M), and porosity parameter (K) on temperature and velocity profiles are discussed. Nusselt number (Nu) and skin friction coefficient (C_f) are evaluated. Significant results of present research are outlined as follows:

- Velocity of nanofluid decelerates with increase in porosity and magnetic parameter.
- Temperature and velocity profile increases as nanoparticle volume fraction enlarges.
- Small values of Nusselt number are obtained corresponding to heat generation or absorption coefficient as well as thermal radiation parameter.
- Observations claimed that for rising values of porosity parameter, absolute values of skin friction coefficient accelerates .
- Temperature of nanofluid enhances for escalating values of radiation parameter and heat generation or absorption coefficient.

Bibliography

- [1] Choi, S US and Eastman, Jeffrey A. (1995). Enhancing thermal conductivity of fluids with nanoparticles. *Argonne National Lab., IL (United States)*.
- [2] Khanafer, Khalil and Vafai, Kambiz and Lightstone, Marilyn. (2003). Buoyancy-driven heat transfer enhancement in a two-dimensional enclosure utilizing nanofluids. *International journal of heat and mass transfer*, **46(19)**, 3639–3653.
- [3] Buongiorno, Jacopo. (2006). Convective transport in nanofluids. **128**, 240–250.
- [4] Akbar, Noreen Sher and Nadeem, Sohail. (2013). Mixed convective magnetohydrodynamic peristaltic flow of a Jeffrey nanofluid with Newtonian heating. *Zeitschrift für Naturforschung A*, **68(6-7)**, 433–441.
- [5] Khan, ZH and Hussain, ST and Hammouch, Z and others. (2016). Flow and heat transfer analysis of water and ethylene glycol based Cu nanoparticles between two parallel disks with suction/injection effects. *Journal of Molecular Liquids*, **221**, 298–304.
- [6] Saleem, S and Nadeem, S and Haq, Rizwan Ul. (2014). Buoyancy and metallic particle effects on an unsteady water-based fluid flow along a vertically rotating cone. *The European Physical Journal Plus*, **129(10)**, 1–8.

- [7] Ibrahim, Wubshet and Haq, Rizwan Ul. (2016). Magneto hydrodynamic (MHD) stagnation point flow of nanofluid past a stretching sheet with convective boundary condition. *Journal of the Brazilian Society of Mechanical Sciences and Engineering*, **38(4)**, 1155–1164.
- [8] Hussain, ST and Khan, ZH and Nadeem, S and others. (2016). Water driven flow of carbon nanotubes in a rotating channel. *Journal of Molecular Liquids*, **124**, 136–144.
- [9] Rassoulinejad-Mousavi, Seyed Moein and Yaghoobi, Hessameddin. (2014). Effect of non-linear drag term on viscous dissipation in a fluid saturated porous medium channel with various boundary conditions at walls. *Arabian Journal for Science and Engineering*, **39(2)**, 1231–1240.
- [10] Vardanyan, VA. (1973). Effect of magnetic field on blood flow. *Biofizika*, **18**, 491–496.
- [11] Richardson, EG and Tyler, E. (1929). The transverse velocity gradient near the mouths of pipes in which an alternating or continuous flow of air is established. *Proceedings of the Physical Society (1926-1948)*, **42(1)**, 1.
- [12] Atabek, H Bülent and Chang, Chieh C. (1961). Oscillatory flow near the entry of a circular tube. *Zeitschrift für angewandte Mathematik und Physik ZAMP*, **12(3)**, 185–201.
- [13] Sucec, James. (1981). An improved quasi-steady approach for transient conjugated forced convection problems. *International Journal of Heat and Mass Transfer*, **24(10)**, 1711–1722.

- [14] Chaturani, P and Palanisamy, V. (1990). Pulsatile flow of power-law fluid model for blood flow under periodic body acceleration. *Biorheology*, **27(5)**, 747–758.
- [15] El-Shahed, Moustafa, (2003). Pulsatile flow of blood through a stenosed porous medium under periodic body acceleration. *Applied Mathematics and Computation*, **138(2-3)**, 479–488.
- [16] Majdalani, Joseph and Chibli, Hicham. (2002). Pulsatory channel flows with arbitrary pressure gradients. *3rd Theoretical Fluid Mechanics Meeting*, 2981.
- [17] Yakhot, Alexander and Grinberg, Leopold. (2003). Phase shift ellipses for pulsating flows. *Physics of Fluids*, **15(7)**, 2081–2083.
- [18] Sanyal, Dulal Chandra and Biswas, Ananda. (2010). Pulsatile motion of blood through an axi-symmetric artery in presence of magnetic field. *Assam University Journal of Science and Technology*, **5(2)**, 12–20.
- [19] Shahzad, Faisal and Haq, Rizwan Ul and Al-Mdallal, Qasem M. (2016). Water driven Cu nanoparticles between two concentric ducts with oscillatory pressure gradient. *Journal of Molecular Liquids*, **224**, 322–332.
- [20] Bansal, JL. (1994). Magnetofluidynamics of viscous fluids. *Jaipur Publishing House*.
- [21] Crane, Lawrence J. (1970). Flow past a stretching plate. *Zeitschrift für angewandte Mathematik und Physik ZAMP*, **21(4)**, 645–647.
- [22] Miklavčič, M and Wang, C. (2006). Viscous flow due to a shrinking sheet. *Quarterly of Applied Mathematics*, **64(2)**, 283–290.

- [23] Wang, CY. (1990). Liquid film on an unsteady stretching surface. *Quarterly of Applied Mathematics*, **48(4)**, 601–610.
- [24] Fang, Tiegang and Zhang, Ji. (2009). Closed-form exact solutions of MHD viscous flow over a shrinking sheet. *Communications in Nonlinear Science and Numerical Simulation*, **14(7)**, 2853–2857.
- [25] Pavlov, KB. (1974). Magnetohydrodynamic flow of an incompressible viscous fluid caused by deformation of a plane surface. *Magnitnaya Gidrodinamika*, **4(1)**, 146–147.
- [26] Ishak, Anuar and Jafar, Khamisah and Nazar, Roslinda and Pop, Ioan. (2009). MHD stagnation point flow towards a stretching sheet. *Physica A: Statistical Mechanics and its Applications*, **388(17)**, 3377–3383.
- [27] Rudraiah, N and Barron, RM and Venkatachalappa, M and Subbaraya, CK. (1995). Effect of a magnetic field on free convection in a rectangular enclosure. *International Journal of Engineering Science*, **33(8)**, 1075–1084.
- [28] Kumaran, V and Kumar, A Vanav and Pop, I. (2010). Transition of MHD boundary layer flow past a stretching sheet. *Communications in Nonlinear Science and Numerical Simulation*, **15(2)**, 300–311.
- [29] Prasad, Vishwanath and Kulacki, FA. (1984). Natural convection in a vertical porous annulus. *International journal of heat and mass transfer*, **27(2)**, 207–219.
- [30] Yih, KA. (1999). Radiation effect on natural convection over a vertical cylinder embedded in porous media. *International communications in heat and mass transfer*, **26(2)**, 259–267.

- [31] Badruddin, Irfan Anjum and Zainal, ZA and Khan, Zahid A and Mallick, Zulquernain. (2007). Effect of viscous dissipation and radiation on natural convection in a porous medium embedded within vertical annulus. *International journal of thermal sciences*, **46(3)**, 221–227.
- [32] Butt, Adnan Saeed and Ali, Asif and Mehmood, Ahmer. (2016). Numerical investigation of magnetic field effects on entropy generation in viscous flow over a stretching cylinder embedded in a porous medium. *Energy*, **99**, 237–249.
- [33] Ahmed, Sameh E and Hussein, Ahmed Kadhim and Mohammed, Hussein A and Sivasankaran, S. (2014). Boundary layer flow and heat transfer due to permeable stretching tube in the presence of heat source/sink utilizing nanofluids. *Applied Mathematics and Computation*, **238**, 149–162.
- [34] Ishak, Anuar and Nazar, Roslinda and Pop, Ioan. (2008). Uniform suction/blowing effect on flow and heat transfer due to a stretching cylinder. *Applied Mathematical Modelling*, **32(10)**, 2059–2066.
- [35] Ashorynejad, HR and Sheikholeslami, M and Pop, I and Ganji, DD. (2013). Nanofluid flow and heat transfer due to a stretching cylinder in the presence of magnetic field. *Heat and Mass Transfer*, **49(3)**, 427–436.
- [36] Ishak, Anuar and Nazar, Roslinda and Pop, Ioan. (2008). Magnetohydrodynamic (MHD) flow and heat transfer due to a stretching cylinder. *Energy Conversion and Management*, **49(11)**, 3265–3269.
- [37] Sheikholeslami, M and Gorji-Bandpy, M and Ganji, DD and Soleimani, Soheil. (2013). Effect of a magnetic field on natural convection in an inclined half-annulus

- enclosure filled with Cu–water nanofluid using CVFEM. *Advanced Powder Technology*, **24(6)**, 980–991.
- [38] Sheikholeslami, M and Ganji, DD and Ashorynejad, HR and Rokni, Houman B. (2012). Analytical investigation of Jeffery-Hamel flow with high magnetic field and nanoparticle by Adomian decomposition method. *Applied Mathematics and Mechanics*, **33(1)**, 25–36.
- [39] Domairry, Davood and Sheikholeslami, Mohsen and Ashorynejad, Hamid Reza and Gorla, Rama Subba Reddy and Khani, Mostafa. (2011). Natural convection flow of a non-Newtonian nanofluid between two vertical flat plates. *Proceedings of the Institution of Mechanical Engineers, Part N: Journal of Nanoengineering and Nanosystems*, **225(3)**, 115–122.
- [40] Ashorynejad, Hamid Reza and Mohamad, Abdulmajeed A and Sheikholeslami, Mohsen. (2013). Magnetic field effects on natural convection flow of a nanofluid in a horizontal cylindrical annulus using Lattice Boltzmann method. *International Journal of Thermal Sciences*, **64**, 240–250.
- [41] Tiwari, Raj Kamal and Das, Manab Kumar. (2007). Heat transfer augmentation in a two-sided lid-driven differentially heated square cavity utilizing nanofluids. *International Journal of heat and Mass transfer*, textbf50(9-10), 2002–2018.
- [42] Wang, CY. (1988). Fluid flow due to a stretching cylinder. *The Physics of fluids*, **31(3)**, 466–468.
- [43] Shampine, Lawrence F and Kierzenka, Jacek and Reichelt, Mark W and others. (2000). Solving boundary value problems for ordinary differential equations in MATLAB with bvp4c. *Tutorial notes*, **2000**, 1–27.

- [44] Gökhan, Fikri Serdar. (2011). Effect of the guess function & continuation method on the run time of matlab bvp solvers. *Edited by Clara M. Ionescu*, **1**.
- [45] Aminossadati, S. M., & Ghasemi, B. (2009). Natural convection cooling of a localised heat source at the bottom of a nanofluid-filled enclosure. *European Journal of Mechanics-B/Fluids*, **28(5)**, 630–640.
- [46] Pandey, Alok Kumar and Kumar, Manoj. (2017). Natural convection and thermal radiation influence on nanofluid flow over a stretching cylinder in a porous medium with viscous dissipation. *Alexandria Engineering Journal*, **56(1)**, 55–62.
- [47] Manjunatha, PT and Gireesha, BJ and Prasannakumara, BC. (2017). Effect of radiation on flow and heat transfer of MHD dusty fluid over a stretching cylinder embedded in a porous medium in presence of heat source. *International Journal of Applied and Computational Mathematics*, **3(1)**, 293–310.
- [48] Sheikholeslami, Mohsen. (2015). Effect of uniform suction on nanofluid flow and heat transfer over a cylinder. *Journal of the Brazilian Society of Mechanical Sciences and Engineering*, **37(6)**, 1623–1633.

Appendix

Table 6.1: Dimensions

Quantity	Symbols	Dimension
Time	t	$[T]$
Velocity	v	$[LT^{-1}]$
Pressure	p	$[ML^{-1}T^{-2}]$
Viscosity	μ	$[ML^{-1}T^{-1}]$
Density	ρ	$[ML^{-3}]$
Kinematic viscosity	ν	$[L^2T^{-1}]$
Dynamic viscosity	μ	$[ML^{-1}T^{-1}]$
Force	F	$[MLT^{-2}]$
Specific heat	c_p	$[L^2T^{-2}K^{-1}]$
Thermal diffusivity	α	$[L^2T^{-1}]$
Thermal conductivity	κ	$[MLT^{-3}K^{-1}]$
Electrical conductivity	σ	$[M^{-1}L^{-3}T^3I^2]$
Temperature	T	$[K]$
Stefan-Boltzmann constant	σ^*	$[MT^{-3}K^{-4}]$
Magnetic field	B	$[MT^{-2}I^{-1}]$
Mean absorption	k^*	$[L^{-1}]$
Current density	J	$[IL^{-2}]$
Lorentz force	F_L	$[LMT^{-2}]$
Electric field	E	$[MLT^{-3}I^{-1}]$
Positive constant	b	$[T^{-1}]$
Permeability	K_o	$[L^2]$